Quantum dimer model with extensive ground-state entropy on the kagome lattice

G. Misguich,* D. Serban,† and V. Pasquier‡
Service de Physique Théorique, CEA Saclay, 91191 Gif-sur-Yvette Cedex, France
(Received 7 February 2003; published 10 June 2003)

We introduce a quantum dimer model on the kagome lattice with kinetic terms allowing from three to six dimers to resonate around hexagons. Unlike the models studied previously, the different resonance loops appear with different *signs* (given by the parity of the number of dimers involved). These signs naturally appear when performing the lowest-order overlap expansion (Rokhsar and Kivelson 1988) of the Heisenberg model. We demonstrate that the quantum dimer model has an extensive zero-temperature entropy and has very short-range dimer-dimer correlations. We discuss the possible relevance of this kind of quantum dimer liquid to the physics of the spin-$\frac{1}{2}$ Heisenberg model on the kagome lattice.

DOI: 10.1103/PhysRevB.67.214413 PACS number(s): 75.10.Jm, 75.50.Ee

I. INTRODUCTION

Quantum frustrated Heisenberg antiferromagnets are fascinating systems that can display a vast variety of exotic phases and phenomena. Systems with strong quantum fluctuations where no magnetic long-range order develops down to zero temperature (''spin liquids'' loosely speaking) are of particular interest because they do not have direct classical analogs and are strongly interacting problems that resist many simple theoretical approaches. Focusing on two dimensions and spin-$\frac{1}{2}$, two kinds of magnetically disordered phases are well understood: valence-bond crystal (VBC) and short-range resonating valence-bond (RVB) liquids. Both are characterized by short-ranged spin-spin correlations but the VBC has long-ranged singlet-singlet correlations and gapped spin-1 excitations whereas the RVB liquid has short-ranged singlet-singlet correlations, topological order, and spin-$\frac{1}{2}$ (spinon) excitations.

Despite intense theoretical efforts,[1–16] the physics of the spin-$\frac{1}{2}$ kagome[17] antiferromagnetic Heisenberg model (KAFH) is still debated. For instance, there is still no consensus on the mechanisms that produce the unusually large density of singlet states that was observed numerically.[13,14]

Quantum dimer models[18,19] (QDM) are effective approaches to the phases of antiferromagnets which are dominated by short-range valence bonds. These models are defined in the Hilbert space of nearest-neighbor valence bond (or dimer) coverings of the lattice and contain kinetic- as well as potential-energy terms for these dimers. These models can often be simpler than their spin parents and are amenable to several analytic treatments because of their close relations to classical dimer problems,[20] Ising models, and $\mathbb{Z}_2$ gauge theory.[19,21,22] These models can offer simple descriptions of VBC (Ref. 18) as well as RVB liquids[23,21] and a natural question is whether QDM can describe other phases, and, in particular, whether they can describe phases with *gapless singlet excitations*. Motivated by the problem of the spin-$\frac{1}{2}$ KAFH, we investigated some QDM on the kagome lattice. Because of the corner-sharing triangle geometry, dimer coverings can be handled in a much simpler way (with pseudospin variables[5,21]) than on other lattices. Exploiting this property we introduce a QDM (called the μ model thereafter) with several interesting properties.

(i) The Hamiltonian allows dimers (from three to six at a time) to resonate around hexagons with amplitudes that have nontrivial *signs*. These signs are those arising when performing the lowest-order expansion (in the dimer overlap parameter introduced by Rokhsar and Kivelson,[18] see Sec. IV) of the KAFH Hamiltonian in the valence-bond subspace.[6] These signs are the crucial difference with the solvable QDM we introduced previously.[21] For this reason also quantum Monte Carlo simulations would face the well-known sign problem.

(ii) In addition to the topological degeneracy, a feature of dimer liquids, the ground state has a degeneracy which is exponential with the number of sites, that is, an *extensive zero-temperature entropy*.

(iii) The ground states have short-ranged dimer-dimer correlations, they are *dimer liquids*. We studied the model through simple mean-field approximations as well as numerically and we propose a picture in which the system is critical (or at least close to a critical point).

Because some parts of the paper are relatively independent, we will now summarize it so that readers may directly go to a specific part. In Sec. II we review some results on the KAFH model. Although this paper is mostly devoted to a *dimer* model (sort of extreme quantum limit of the SU(2) spin-$\frac{1}{2}$ model), we find it useful to review well established facts concerning the *spin* (Heisenberg) model and we motivate the QDM approach to the KAFH. In particular, in Sec. II F, we present numerical results (spectrum and specific heat) obtained by diagonalizing exactly (on finite-size systems) the Heisenberg model restricted to nearest-neighbor valence-bonds subspace. In Sec. III we discuss general properties of dimer coverings on lattices made of corner-sharing triangles. These properties (existence of pseudospin variables and their dual representation in terms of arrows) turn out to be useful to define and analyze QDM on these lattices, including kagome. In Sec. IV we explain the Rokhsar-Kivelson overlap expansion when applied to the family of lattices mentioned above. At lowest order the kinetic-energy terms have signs depending on the parity of the number of dimers involved. Ignoring the amplitudes and keeping only these signs (Sec. V), we get kinetic (i.e., nondiagonal) dimer operators $\mu(h)$ defined on every hexagon h of kagome and which realize an original algebra: (i) $\mu(h)^2=1$, (ii) they anti-

 ©2003 The American Physical Society

commute on neighboring hexagon, and (iii) commute otherwise. The rest of the paper is devoted to the analysis of the Hamiltonian defined as the sum of all the $\mu(h)$. In Sec. V D we start by solving exactly the dimer model on a one-dimensional lattice. It sustains critical (algebraic) correlations and has an extensive zero-temperature entropy. Although we did not succeed in finding an exact solution to it, we were able to show (Sec. V E) that the kagome μ model also have such a zero-temperature entropy. Some mean-field treatments are discussed in Sec. V E 3 and a competing crystal-like phase is identified. In Sec. V E 7 we introduce fermionic variables dual to the μ operators, in which the residual entropy is quite transparent. This formulation is reminiscent of the $\mathbb{Z}_2$ gauge theory in Ref. 21. The last section (VI) is devoted to numerical calculations on the kagome μ model.

II. SOME RESULTS ON THE KAGOME HEISENBERG ANTIFERROMAGNET

In this section we review a few results concerning the Heisenberg model on the kagome lattice.

A. Classical degeneracy

The classical kagome antiferromagnet attracted interest because of its unusual low-temperature properties. These properties are related to the existence of a local and continuous degeneracy. Indeed, any spin configuration, that has a vanishing total magnetization $\vec{S}_1+\vec{S}_2+\vec{S}_3=\vec{0}$ on every triangle, minimizes the Heisenberg energy. Counting *planar ground states* amounts to finding the number of ways one can put *A*, *B*, and *C* on the lattice so that each triangle has spins along the three different orientations. This already represents an extensive entropy.[24–26] In a given planar ground state, one can look for closed loops of type $A-B-A-B-\cdots$. Because, on kagome, such a loop has only *C*-type neighbors, rotating the spins of this loop around the *C* axis costs no energy and gives new (nonplanar) ground states. Chalker *et al.*[27] showed that all ground states can be obtained by repeated introduction of such distortions into the different parent planar states.[28] At low temperature this classical spin system has no magnetic long-range order (LRO) but exhibits diverging *nematic* correlations when the temperature goes to zero: although spin-spin correlations are short ranged, the planes defined by the three spins of a triangle are correlated at long distances. This phenomenon is a manifestation of ''order by disorder'': thermal fluctuations select ground states with the largest number of soft modes and these are the planar ground states.

B. Absence of Néel long-range order

It has been known for some time that the spin-$\frac{1}{2}$ kagome Heisenberg antiferromagnet has no Néel LRO at zero temperature. Early spin-wave calculations by Zeng and Elser[2] indicated that magnetic order disappears when going from the triangular antiferromagnet to the kagome model. This was supported by numerical calculations of spin-spin correlations in finite kagome clusters up to 21 sites.[2] Two years later, Singh and Huse[4] performed a series expansion about an Ising limit and came to the same conclusion about the absence of magnetic LRO.

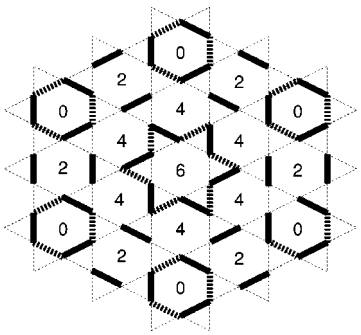

FIG. 1. Crystal of resonating hexagons (marked with 0) on the kagome lattice. Labels $n=0,2,4,6$ correspond to the possible resonance loop L_n around each hexagon according to Table I.

Although the classical model has no Néel LRO at $T=0$, the absence of such an order in the spin-$\frac{1}{2}$ case is not completely trivial because quantum fluctuations could select a particular type of ground state. Sachdev[8] showed in the context of a large-*N* expansion that for a large enough value of the ''spin,'' a Néel LRO sets in (the so-called $\sqrt{3}\times\sqrt{3}$ structure).

In 1993 Leung and Elser[9] pushed exact diagonalizations to 36 spins and confirmed the absence of Néel LRO. They also studied four-spin correlations (dimer-dimer) to investigate the issue of a possible valence-bond crystal (or spin-Peierls, or bond-ordered) phase made of resonating hexagons (see Fig. 1). They found very weak correlations and suggested the existence of a liquid phase (they could not, however, definitely rule out the possibility of a very weak crystalline LRO order). Nakamura and Miyashita[11] did Monte Carlo simulations including $N=36$ and $N=72$ spins, which showed no kind of spin or dimer ordering down to $T\simeq 0.2J$ (Ref. 29) but found a low-temperature peak in the specific heat.

On the analytical side, Sachdev[8] generalized the SU(2) model to an Sp($2N$) symmetry and worked out a large-*N* approach based on bosonic representations. He found a quantum ordered phase with no broken symmetries and unconfined bosonic spinons. However, this result does not directly explain[30] the huge density of low-energy singlet states that was observed numerically and that we discuss below.

C. Low-energy singlet states

Lecheminant *et al.*[13] and Waldtmann *et al.*[14] calculated a large number of low-energy eigenstates for finite kagome clusters up to 36 sites. These results pointed to a large ''residual'' entropy at low temperatures. From their data the residual entropy per site can be estimated to be $s_0\sim 0.2\ln(2)$. This number was obtained by counting the number of eigenstates in a finite (and nonextensive)-energy window above the ground state. This number was found to scale as $\sim\alpha^N$ with $\alpha\simeq 1.15$. The width of this energy window is expected to modify numerical prefactors[31] but not α which is directly related to the entropy per site $s_0=\ln(\alpha)$.

D. Specific heat

The entropy change between zero and infinite temperature can be extracted from the specific heat $c_v(T)$. The first high-temperature (HT) series expansion for the kagome antiferromagnet was carried out by Elstner and Young.[10] This approach showed a huge entropy deficit of about 40%: $\int_0^\infty c_v(T)/TdT \simeq 0.6\ln(2)$. However, this direct evaluation of the specific heat from the HT series is not accurate at low temperatures and they concluded the possibility of a low-temperature peak in the specific heat. A quantum Monte Carlo simulation by Nakamura and Miyashita[11] also found a low-temperature peak. Such a peak was also found by a decimation calculation.[12] A recent exact diagonalization work by Sindzingre *et al.*[32] also found such a peak in a 36-sites sample. An improved method of calculating $c_v(T)$ from high-temperature series expansion, which is quantitatively accurate down to zero temperature in most frustrated magnets,[33] shows that about 20% of the total entropy is still missing at very low temperatures,[34] in agreement with exact diagonalizations data.

E. Residual entropy

If a system has a number of states growing exponentially (with the system size) in a non-extensive energy window above the ground state, it has an extensive residual entropy at zero temperature. In such a case, although the ground state can be unique on finite systems, it is, in fact, exponentially degenerate in the thermodynamic sense.[35] One can construct some simple models with an extensive residual entropy (the Ising antiferromagnet on the triangular lattice for instance) but it is usually lifted by almost any infinitesimally small perturbation. An extensive entropy at $T=0$ is not a generic situation, but instead requires some fine tuning (to zero) of all these perturbations. For these reasons we think it is unlikely that the spin-$\frac{1}{2}$ kagome Heisenberg antiferromagnet has a $T=0$ residual entropy. Consider some Hamiltonian $\mathcal{H}(\lambda)=\mathcal{H}_0+\lambda\mathcal{H}_1$, where $\mathcal{H}_0$ has an exponential ground state degeneracy which is lifted by $\mathcal{H}_1$. At small λ the specific heat may have a low-temperature peak whose entropy corresponds to the ground state degeneracy of $\mathcal{H}_0$. Upon taking the $\lambda\to 0$ limit, the temperature of the peak goes to zero as well. This is the picture we have in mind for the spin-$\frac{1}{2}$ kagome antiferromagnet and this paper discusses a possible scenario in which the role of $\mathcal{H}_0$ is played by a quantum dimer model (defined as the μ model in Sec. V).

F. Resonating valence-bond subspace

Quantum dimer models can provide effective descriptions of some magnetically disordered phases of antiferromagnets. We first wish to motivate the restriction of the spin Hilbert space to the first-neighbor RVB subspace that has been used in a number of works[5,6,15,36] for the kagome problem. This space is generated by all valence-bond states where spins are paired into first-neighbor singlets (dimers or valence bond). Because spin-spin correlations are very short ranged, it is rather natural to consider the ground-state wave function as a linear superposition of valence-bond states. The crucial point is to understand whether valence bonds beyond first neighbors should be included or not in the Hilbert space to get (qualitatively) the right physics. We will only partially address this in this paper. This first-neighbor RVB limit is the simplest subspace that has an exponential number of states that could explain the proliferation of low-energy singlets observed numerically. In addition, this subspace provides a reasonably good variational energy. Zeng and Elser[6] and Mambrini and Mila[36] computed the ground-state energy of the Heisenberg Hamiltonian restricted to the first-neighbor RVB subspace.[37] For a sample of 36 sites, their result ($2\langle\vec{S}_i\cdot\vec{S}_j\rangle=-0.4218$) is 3.8% higher than the exact ground-state energy obtained[9,14] in the full spin Hilbert space ($2\langle\vec{S}_i\cdot\vec{S}_j\rangle=-0.4384$). Zeng and Elser were able to improve significantly this variational estimate by a simple optimization of the dimer wave function in the vicinity of each defect triangle, but without changing the dimension of the Hilbert space. To our knowledge, this ''optimized dimerizations basis'' is the best variational one for the kagome problem. It is also worth saying that in the fermionic large-N extension of the Heisenberg model, first-neighbor valence-bond states arise as degenerate ground states in the $N\to\infty$ limit.[38] $1/N$ corrections will then introduce a dynamics among these dimerized states. Marston and Zeng[7] used such a fermionic SU(N) extension of the Heisenberg model on the kagome lattice and found that such $1/N$ corrections could favor the crystal of resonating hexagons mentioned above (Fig. 1).

A last argument for the first-neighbor RVB approach to the kagome problem is the fact that the spectra of the Heisenberg model projected into this subspace reproduce a continuum of singlet states as in the case of spectra computed in the full spin Hilbert space. This was first noticed by Mambrini and Mila[36] on samples up to 36 spins and we extended their study to samples up to 48 sites. Figure 2 shows the

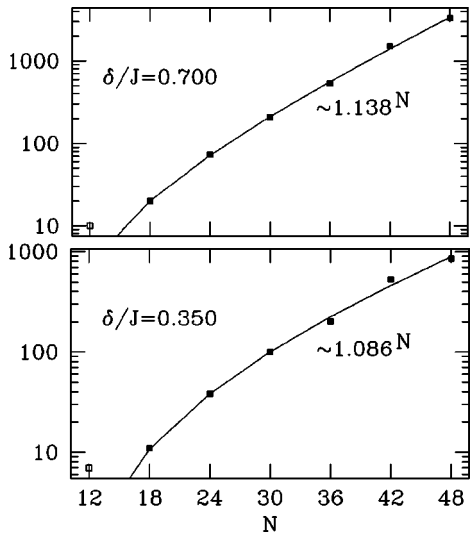

FIG. 2. Kagome Heisenberg antiferromagnet diagonalized in the first-neighbor RVB space. An exponential number of eigenstates is observed in the energy window $[E_0, E_0+\delta]$, where E_0 is the ground-state energy. The results for two values of δ are shown. The full lines are quadratic least-square fits to the data for $N\geqslant 18$. The definition of J is such that $\mathcal{H}=\Sigma_{\langle i,j\rangle}\vec{S}_i\cdot\vec{S}_j$.

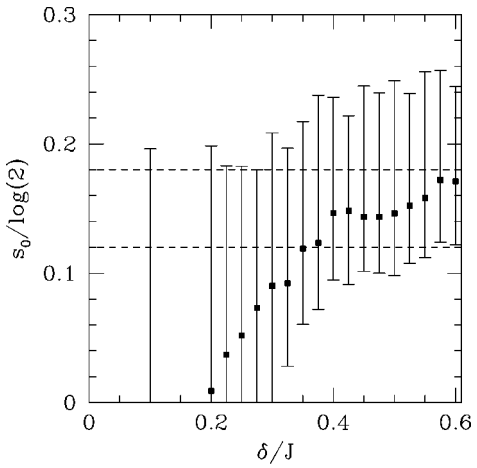

FIG. 3. For each width δ of the energy window we fit the exponential increase of the number of energy levels to estimate the zero-temperature entropy s_0 (as in Fig. 2). Error bars come from the uncertainty of the least-square fits.

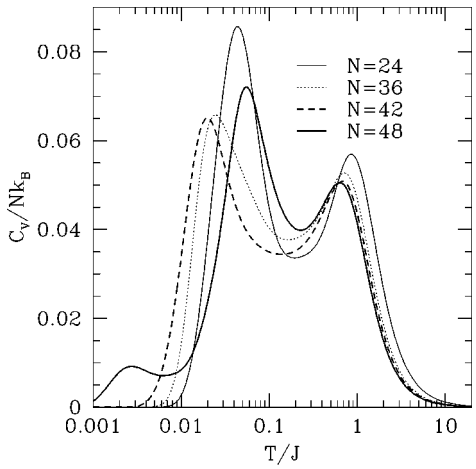

FIG. 4. Specific heat per site of the kagome Heisenberg model restricted to the first-neighbor RVB subspace. The lowest peak at $T/J \simeq 3.10^{-3}$ ($N=48$) is a finite-size artifact.

exponential number of low-energy states in a finite-energy window $[E_0, E_0+\delta]$ above the ground state. We analyzed this exponential proliferation of energy levels as a function of the system size *and* as a function of the energy window. Although we have seven complete spectra up to $N=48$ sites, the dependence on the width of the energy window makes it difficult to give a precise estimate of the low-temperature entropy. For each value of δ we plot the logarithm of the number of states in the window as in Fig. 2. A (least-square) fit is performed to extract the leading exponential behavior when $N \to \infty$. Error bars are obtained in a standard way.[39] In principle, this procedure measures the zero-temperature entropy provided that $\delta/J \ll N$. The result is summarized in Fig. 3. Unfortunately, one cannot use too small values of δ because discretization effects scatter the data when δ is of the same order as the typical level spacing in the smallest samples. This is the reason for the increasingly large error bars we obtain when δ is below $0.6 \sim 0.8J$ (Fig. 3). However, from these results it appears likely that a significant part of the total entropy is present at temperatures much lower than the energy scale J. Indeed, the values of s_0 compatible with the set of data displayed in Fig. 3 are $0.1\ln(2) \leqslant s_0 \leqslant 0.2\ln(2)$. Only these values are within the error bars of all estimates from $\delta = 0.4J$ to $\delta = 1.2J$.

Computing the specific heat is another method to look for a possible residual entropy. In the case of the kagome antiferromagnet diagonalized in the full spin Hilbert space a low-temperature peak was observed,[32] as well as in some experiment on a spin-$\frac{3}{2}$ kagome compound.[40] From its low sensitivity to an applied magnetic field, this peak was attributed (mostly) to nonmagnetic singlet states. In this work we computed the specific heat of the kagome antiferromagnet in the first-neighbor RVB subspace. This calculation is done from the spectra obtained by numerical diagonalizations up to $N=48$ sites. The results are shown in Fig. 3. The maximum of $C_V(T)$ around $T=0.7J$ is almost converged to its thermodynamic limit. It corresponds to the onset of short-range correlations. For all sample sizes, a large low-temperature peak is present at or below $T=0.07J$. It is still size dependent but its entropy roughly corresponds to one-half of the total entropy of the model [the total entropy per site of the RVB space is $\frac{1}{3}\ln(2)$], in agreement with the results of Fig. 4. The similarity between these results and those obtained in the full spin Hilbert space is another support to the RVB approach.

To summarize, we have reviewed several arguments indicating that the unusual low-temperature peak in the specific heat of the kagome antiferromagnet might be explained within the framework of a RVB space. We would like to conclude this section by mentioning that the spin-$\frac{1}{2}$ Heisenberg model may have a large number of low-energy singlet states on other lattices made of corner-sharing triangles. This was observed numerically[41] on the frustrated three-leg ladder shown in Fig. 9. We will come back to that model in Sec. V D. In Ref. 42 the squagome lattice was introduced and some low-energy states, reminiscent of the kagome ones, were identified in a large-N approach. A decimation method applied to this lattice also predicts a low-temperature peak in the specific heat of the model.[43] A numerical diagonalization study of the Heisenberg antiferromagnet on the Sierpinski gasket[44] found a low-temperature peak in the specific heat as well.

III. DIMER COVERINGS ON LATTICES MADE OF CORNER-SHARING TRIANGLES

Before studying the restriction of the Heisenberg spin model to the valence-bond subspace, we will introduce some properties of dimer coverings on lattices made of corner-sharing triangles (including kagome). A very useful property discovered by Elser and Zeng[5] is that dimer coverings on these lattices can be put in one-to-one correspondence with configurations of arrow variables. Also, this representation is intimately connected to the existence of (Ising-like) pseudospin variables.[21]

The correspondence between dimer coverings on the

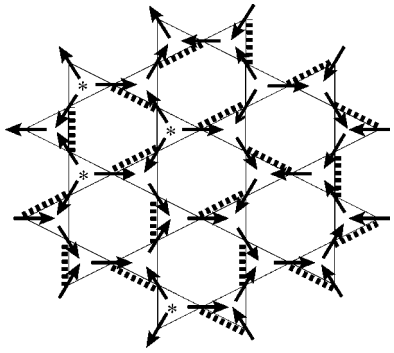

FIG. 5. Arrow representation of a dimer coverings.

kagome lattice and *sets of arrows* is illustrated in Fig. 5. Each arrow has two possible directions: it must point toward the interior of one of the two neighboring triangles. In a triangle, a dimer connects two sites where the arrows point inwards. In a defect triangle (without any dimer, marked with * in Fig. 5), the three arrows point outwards. Therefore, at each triangle there is a constraint imposing that the number of incoming arrows is even.

Dimer moves translate very simply in the arrow representation. One can easily verify that $\sigma^x(h)$ (see Ref. 21 and Appendix A) does nothing but flip the six arrows sitting around hexagon h and that such an operation conserves the constraint for all triangles. Any dimer move[45] is a product $\sigma^x(h_1)\sigma^x(h_2)\ldots$, where $h_1, h_2, \ldots$ are the hexagons enclosed in the loops. This operation successively flips all the arrows around $h_1, h_2, \ldots$. The result does not depend on the order in which hexagons are flipped, so the σ^x operators obviously commute in this language.

A. Medial lattice construction

The arrow representation (as well as the pseudospin operators σ^x and σ^z introduced by Zeng and Elser[5,6]—see Appendix A) can be generalized to all lattices made by corner-sharing triangles. The kagome case is the simplest example in two dimension, another being the squagome lattice[42] (Fig. 8). The Sierpinski gasket[44] is an example of fractal structure of dimension between 1 and 2 also made by corner-sharing triangles.

(a) Start with a trivalent lattice H, that is a lattice where each site has three neighbors (full lines in Figs. 6–10). The hexagonal lattice (Fig. 7) is the simplest two-dimensional example.

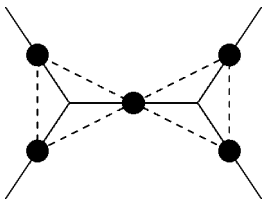

FIG. 6. Medial lattice construction. Starting from a trivalent lattice (full lines) we construct a lattice whose sites (black dots) are centers of the links. The sites of this new lattice are linked together (dashed lines) to form triangular plaquettes.

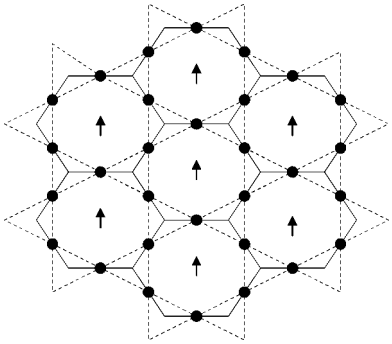

FIG. 7. Kagome lattice (dashed lines and black dots) constructed as the medial lattice of the hexagonal (full lines) lattice. The locations of the pseudospins are indicated by up spins.

(b) *Construct its medial lattice K*. Sites of K are, by definition, the centers of the links of H. The sites sitting on the three links of H connected to the same site of H are connected together. The medial lattice of the hexagonal lattice is the kagome lattice. Since H is trivalent, K is made of corner-sharing triangles.

(c) Associate a pseudospin to each plaquette of H (i.e., to hexagons of the kagome lattice in the example).

In the following, we will use N for the number of sites in K, which is equal to the number of links in H. The number of sites in H will be $2N/3$, which is equal to the number of triangles in K. The number of plaquette (or faces) in H is equal to the number of pseudospins, we write it N_{ps}. For two-dimensional cases we can apply Euler's relation to the lattice H and we find $(2N/3)-N+N_{\mathrm{ps}}=2-2g$ where g is its genus ($g=1$ for a torus, $g=0$ for a sphere).

B. Counting dimer coverings with arrows

The number of dimer coverings of any lattice of type K (including, for instance, the one-dimensional examples of Figs. 9 and 10) is

$$\mathcal{N}_{\text{dim. coverings}}=2^{N/3+1}. \tag{1}$$

This result can be obtained with the arrow representation. Each arrow has two possible directions, which give 2^N states. The fact that there can only be zero or two incoming arrows for each triangle introduces one constraint per tri-

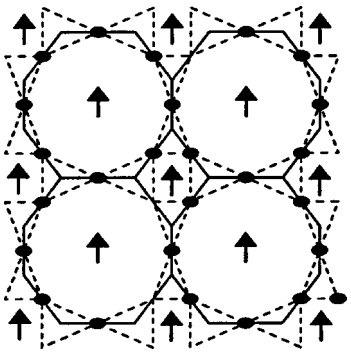

FIG. 8. Squagome lattice (dashed lines) as the medial lattice of the octagonal lattice.

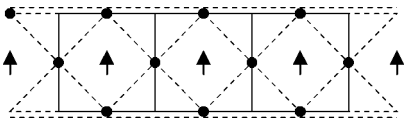

FIG. 9. A frustrated three-spin ladder (dashed lines) obtained as the medial lattice of (trivalent) two-leg ladders.

angle. There are $2N/3$ triangles but only $2N/3-1$ constraints are really independent, which gives Eq. (1).

The fact that $2N/3-1$ constraints are independent can be checked with the following argument. We focus on the trivalent lattice H on the bond of which the arrows live. First transform H into a tree by recursively cutting every bond that does not disconnect the lattice into two parts. The final tree is still trivalent so the number of leaves, L, is related to the number of vertices, V, by $L=V+2$. Each bond gives two leaves when it is cut so that $L/2$ is the number of cuts. One can now set the arrow directions on the leaves. There are $L/2$ such independent arrows. Using the constraints associated with each vertex, the arrows are then determined on all other bonds of the tree by progressively going from the leaves toward the root. It is simple to check that the last constraint encountered when reaching the root is automatically satisfied. From this we obtain $2^{L/2}=2^{V/2+1}$ dimer configurations, which is equivalent to Eq. (1) since $3V=2N$.

IV. FROM SPINS TO DIMERS: OVERLAP EXPANSION

When restricted to the RVB subspace, the Heisenberg model induces a complicated dynamics on valence bonds. This dynamics is intimately related to the nonorthogonality of these valence-bond states, which we describe below.

A. Scalar product and loops

The scalar product of two valence-bond states can be computed from their transition graph[46] (loop covering obtained by drawing both dimerizations on the top of each other). We first need a sign convention for valence-bond states. A simple choice is to orient all the bonds so that all hexagons are clockwise[47] (see Fig. 11). With this choice, the scalar product of two valence-bond states $|a\rangle$ and $|b\rangle$ is

$$\langle a|b\rangle=\prod_{Loops}[(1/2)^{L/2-1}(-1)^{1+N_{\rm hex}+L/2}], \qquad (2)$$

where the product runs over nontrivial (of length >2) loops in the transition graph of a and b, L is the length of the loop, and $N_{\rm hex}$ is the number of hexagons enclosed by a loop. For instance, the loop displayed in Fig. 11 has $N_{\rm hex}=3$. The factor $(1/2)^{L/2-1}$ in Eq. (2) is valid on any lattice whereas the

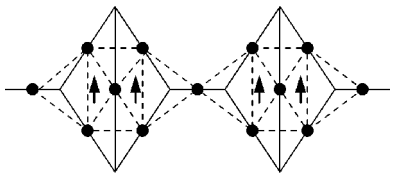

FIG. 10. Another example of chain.

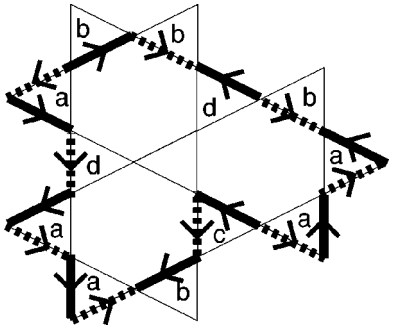

FIG. 11. Transition graph between two dimer coverings. The bonds are oriented so that all hexagons are clockwise. The loop passes through four types of triangles: (a)–(d) (see text).

signs $(-1)^{1+N_{\rm hex}+L/2}$ are associated with the corner-sharing triangle geometry.[48] The sign of $\langle a|b\rangle$ would just be $(-1)^{L/2}$ if all the bond dimers were oriented clockwise around the loops. Consider the triangles on which a loop passes. We classify these triangles in four types (a, b, c and d) as follows. Some have *two* edges on the loop (types a and c in Fig. 11) and the others have only *one* (types b and d). Some are *inside* the loop (types a and d) and the others are *outside* (b and c). Triangles of type a give two counterclockwise bonds and the (-1) factors cancel. Every triangle of type b (c) gives one (resp. two) clockwise bond(s) and does not contribute to the sign. Each triangle of type d gives a counterclockwise bond and contributes by a factor (-1) to the scalar product. Let N_d be the number of such triangles. So far we have shown that $\mathrm{sign}[\langle a|b\rangle]=\Pi_{Loops}(-1)^{N_d+L/2}$. Using the arrow representation (and the associated constraint) one can show that $(-1)^{N_d}=(-1)^{N_{\rm hex}+1}$. The argument—not reproduced here for brevity—uses the fact that the parity of arrows coming out and in of a given cluster of sites is fixed by the number of links and sites in that cluster, and is thus related to the number of hexagons enclosed by the loop.

Rokhsar and Kivelson[18] generalized the scalar product given by Eq. (2) by giving two arbitrary fugacities x and y that couple to the number and to the length of the loops:

$$\langle a|b\rangle_x=\Omega_{xa,b}=\prod_{Loops}[yx^{L/2}(-1)^{1+N_{\rm hex}+L/2}], \qquad (3)$$

x and y can be considered as formal expansion parameters ($x=1/2$, $y=2$ in the physical spin-$\frac{1}{2}$ case). The choice $y=2$ is usually adopted in the literature[6,18] but we will keep y explicit so that other cases may be considered. When $x\to 0$ the overlap matrix Ω_x becomes diagonal.

B. Rokhsar and Kivelson scheme

When restricted to the first-neighbor RVB space, the Heisenberg Hamiltonian induces a dynamics on valence bonds. These valence-bond states are not orthogonal, so we have a generalized eigenvalue problem. Orthogonalized valence bond states $|\tilde{a}\rangle$ can be obtained:

$$|\tilde{a}\rangle = \sum_b (\Omega_x^{-1/2})_{ab} |b\rangle \tag{4}$$

and the matrix to diagonalize is

$$\mathcal{H}^{\rm eff}_{ab}(x) = \langle \tilde{a}|\mathcal{H}|\tilde{b}\rangle_x \tag{5}$$

$$= \sum_{a'b'} (\Omega_x^{-1/2})_{aa'} \langle a'|\mathcal{H}|b'\rangle_x (\Omega_x^{-1/2})_{bb'} \tag{6}$$

where $\mathcal{H}$ is the Heisenberg Hamiltonian, $\mathcal{H} = \Sigma_{\langle ij\rangle} \vec{S}_i \cdot \vec{S}_j$. From now we will only deal with *orthogonalized* valence-bond states $|\tilde{a}\rangle$ but we will drop the tilde for clarity. $\mathcal{H}^{\rm eff}(x=1/2)$ was diagonalized numerically to obtain the results of Fig. 2 and 4 (see also Refs. 6 and 36). $\mathcal{H}_{\rm eff}(x>0)$ is nonlocal and many dimers can hop simultaneously to quite different configurations. However, since $x = \frac{1}{2} < 1$, the tunneling probability for such events decreases exponentially with the loop length. Up to order x^n, $\mathcal{H}^{\rm eff}(x)$ is local and only contains terms with $\leqslant n$ dimers. Following Rokhsar and Kivelson's work on the square lattice,[18] Zeng and Elser[5,6] considered the small-x expansion of $\mathcal{H}^{\rm eff}$ on the kagome lattice up to order x^6. Up to a constant we have

$$\mathcal{H}^{\rm eff}(x) = -\sum_{h,\alpha} h_\alpha(x) |L_\alpha\rangle\langle \overline{L}_\alpha| + {\rm H.c.} + O(x^6) \tag{7}$$

where the sum on h runs over all hexagons, the sum on α runs over all the loops enclosing a that hexagon. The tunneling amplitudes $h_\alpha(x)$ are given in Table I. These results reduce to Zeng and Elser's[6] when $y = 1/x = 2$. Notice that other terms of order x^6 exist and involve six-dimer moves around *two* hexagons.

Equation (7) can be obtained from the scalar product formula. The latter is valid for any lattice K made of corner-sharing triangles (see Sec. III A) and Eq. (7) can be generalized to these lattices. Now hexagons are replaced by plaquettes of lattice H. Consider a loop α encircling a single plaquette. It has a length L and encloses N_t triangles. The amplitude $h_\alpha(x)$ for that dimer move is

$$h_\alpha(x) = \tfrac{1}{2} y (-x)^{L/2} (L - y N_t) + O(x^L_{\rm min}), \tag{8}$$

where $L_{\rm min}$ (equal to 6 for kagome) is the size of the plaquettes of H. Unlike the square[18] or the triangular lattice case,[23] *no sign convention for the dimer coverings can turn the signs of the amplitudes h_α all equal.*

V. QUANTUM DIMER HAMILTONIAN

In Ref. 21 we introduced a solvable model:

$$\mathcal{H}_0 = -\sum_{h,\alpha} |L_\alpha\rangle\langle \overline{L}_\alpha| + {\rm H.c.} = -\sum_h \sigma^x(h), \tag{9}$$

where the pseudospin operators $\sigma^x(h)$ are the kinetic-energy terms defined in Table I (see also Appendix A). This model is obtained by setting $h_\alpha = 1$ in Eq. (7). We showed[21] that Eq. (9) is completely solvable and is the prototype of the RVB dimer liquid. It has a unique ground state (up to a topological degeneracy) and its elementary excitations are pairs of gapped Ising vortices (visons). Here, we search for a model that, as Eq. (9), is amenable to an analytical treatment and that can capture some essential features of the spin model. The first step in treating the frustration inherent to the Heisenberg model on the kagome lattice is to introduce nontrivial *signs* in the dimer resonance loops.

TABLE I. The eight different classes of loops that can surround a hexagon. Including all possible symmetries, we find 32 possible loops. $L/2$ is the number of dimers involved and h_α is the tunneling amplitude (at lowest order) associated with each loop in a small-x expansion of the Heisenberg model in the RVB space (see text). The value for the physical case $y = 1/x = 2$ is given.

Loop α	$L/2$	$h_\alpha(x)$	σ^x	μ	$\tilde{\mu}$
	3	$-3yx^3 = -3/4$	+	-	+
	4	$yx^4(4-y) = 1/4$	+	+	+
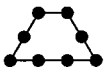	4	$yx^4(4-y) = 1/4$	+	+	-
	4	$yx^4(4-y) = 1/4$	+	+	+
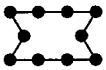	5	$yx^5(2y-5) = -1/16$	+	-	+
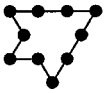	5	$yx^5(2y-5) = -1/16$	+	-	-
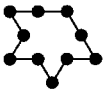	5	$yx^5(2y-5) = -1/16$	+	-	+
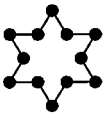	6	$yx^6(6-3y) = 0$	+	+	+

A. Definition of $\mu(h)$

We choose to keep only the sign of the leading terms h_α of the dimer overlap expansion for the Heisenberg model. This leads to the definition of an operator $\mu(h)$ at each pseudospin location h (hexagon centers in the kagome case):

$$\mu(h) = \sum_{\alpha=1}^{32} \epsilon(\alpha) |L_\alpha\rangle\langle \overline{L}_\alpha| + {\rm H.c.} \tag{10}$$

where

$$\epsilon(\alpha) = (-1)^{{\rm Length}(\alpha)/2} \tag{11}$$

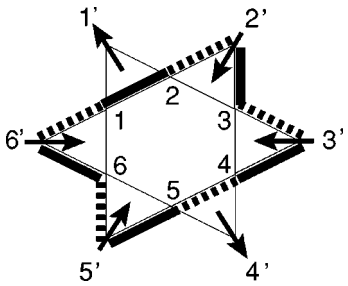

FIG. 12. The position of incoming arrows on sites $1',2',\ldots,$ defines the possible dimer move (full and dashed links) around the hexagon. The arrows at sites $1,2,\ldots,6$ are omitted for clarity; they take opposite directions in the dimerizations pictured by full and dashed dimers, respectively. The arrows at $1',2',\ldots,$ are unchanged during this dimer move.

and Length(α) is the length of the loop α. The action of $\mu(h)$ only differs from the pseudospin flip $\sigma^x(h)$ by a sign: $\mu(h)|D\rangle = \pm\sigma^x(h)|D\rangle$. This sign depends on the length of the admissible loop at h in state $|D\rangle$, as indicated in Table I. With this definition, if $|c\rangle$ is a (nonorthogonalized) dimer configuration, we have $\langle c|\mu(h)|c\rangle \geqslant 0$ for any hexagon h. This can be used to define the signs of the matrix elements of μ independently of the orientation of the dimers.

As for σ^x, μ can be simply expressed in terms of the arrow representation introduced in Sec. III. Let $1,2,\ldots,6$ be the sites of hexagon h and $1',2',\ldots,6'$ be the sites of the ''star'' surrounding this hexagon (see Fig. 12). The length of the admissible loop α_0 around h is related to the state of the arrows on $1',2',\ldots,6'$ in the following way. If the arrow at site i' is pointing toward h, it shares a dimer with a site j belonging to the hexagon and α_0 will pass through i' and j. Let $n_{\rm out}$ be the number of outgoing arrows. From this it is clear that the length of that loop will be Length$(\alpha_0) = 12 - n_{\rm out}$. To summarize, the operator $\mu(h)$ defined in Eq. 10 flips the arrows of sites $1,2,\ldots,6$ and multiplies the configuration by a sign[49]:

$$\epsilon(h) = (-1)^{n_{\rm out}(h)/2}. \tag{12}$$

The operators μ can be explicitly written with the help of σ^z and σ^x operators. Finding such an expression is not completely obvious since σ^z are nonlocal and depend on the reference configuration, whereas μ are local and independent of any reference state. The expression is derived in Appendix B.

B. Commutation rules

1. Operator μ

The μ operators have the remarkable property of (1) anticommuting when they operate on nearest-neighbor hexagons but (2) commuting otherwise. This property is not obvious when looking at Eq. (10) and is most easily demonstrated with the help of the arrow representations. As mentioned previously, the effect of $\mu(h)$ on an arrow configuration is to flip the arrows around hexagon h and multiply it by a sign $\epsilon(h) = (-1)^{n_{out}(h)/2}$. Therefore, the actions of $\mu(A)$ and $\mu(B)$ commute up to a sign. If hexagons A and B are not adjacent, the signs $\epsilon(A)$ and $\epsilon(B)$ are unaffected by the action of $\mu(B)$ and $\mu(A)$, respectively, and $\mu(A)$ and $\mu(B)$ commute. For two neighboring hexagons A and B, the action of $\mu(A)$ affects the sign $\epsilon(B)$ and conversely. There are two types of arrow configuration shared by the neighboring hexagons A and B, as shown in Figs. 13(a) and 13(b). Both configurations have an odd number of outgoing arrows among the four external links, which will be flipped by the successive actions of $\mu(A)$ and $\mu(B)$. One of the signs $\epsilon(A)$ and $\epsilon(B)$ will therefore be changed by the action of the neighboring μ, but not the other. This means that upon acting with $\mu(A)$ and $\mu(B)$, the sign of the final configuration depends on the order we applied the two operators, and we find that on any configuration $\mu(A)\mu(B) = -\mu(B)\mu(A)$.

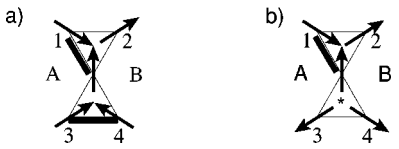

FIG. 13. Two possible states of a pair of triangles.

2. Operator $\tilde{\mu}$

Another choice for the signs of the tunneling amplitudes turns out to be very useful. Consider the $\tilde{\mu}$ operators defined by

$$\tilde{\mu}(h) = \sum_{\alpha=1}^{32} \tilde{\epsilon}(\alpha)|L_\alpha\rangle\langle\overline{L_\alpha}| + \text{H.c.}, \tag{13}$$

where the signs $\tilde{\epsilon}(\alpha)$ are given in the last column of Table I. Contrary to $\epsilon(\alpha)$, $\tilde{\epsilon}(\alpha)$ counts the parity of the number of outgoing arrows only on one-half of the sites of the star: $1'$, $3'$, and $5'$. Using the arrow representation and similar arguments as above, one can show that (1) $\tilde{\mu}$ operators anticommute when acting on nearest-neighbor hexagons (2) commute otherwise. Most interestingly, μ and $\tilde{\mu}$ realize two copies of the same algebra that commute with each other:

$$\forall\ h,h'\ [\mu(h),\tilde{\mu}(h')] = 0. \tag{14}$$

The μ (and $\tilde{\mu}$) operators have simple commutation relations with the pseudospin operators σ^z introduced by Zong and Elser (ZE). By definition, the μ operators can be written as $\mu(h) = \epsilon(h)\sigma^x(h)$, where $\epsilon(h)$ is diagonal operator in the dimer basis. Because σ^z operators are also diagonal in that basis they commute with any ϵ and we simply have $\mu(h)\sigma^z(h) = -\sigma^z(h)\mu(h)$ and $[\mu(h),\sigma^z(h')] = 0$ for $h \neq h'$ (see Appendix A for the commutation rules of σ^x and σ^z operators). The same result holds for $\tilde{\mu}$. In Ref. 21 we identified $\sigma^z(h)$ as the operator that creates (or destroys) an Ising vortex (vison) on hexagon h and a nonzero expectation value $\langle\sigma^z\rangle$ was interpreted as the signature of confinement and vison condensation.

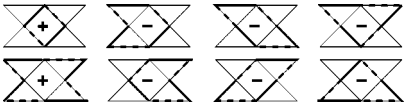

FIG. 14. The eight possible dimer moves around a square plaquette of the frustrated ladder shown in Fig. 9. The signs of the corresponding amplitudes in the μ model are indicated.

C. Hamiltonian

The main results of this paper concern the following quantum dimer model:

$$\mathcal{H}_\mu = -\sum_h \mu(h), \tag{15}$$

where the μ obey the commutation rules described in the preceding section. We studied this model both numerically and analytically. Numerically we diagonalized it on systems up to 144 kagome sites (48 hexagons). The results are presented in Sec. VI. The most striking feature of the spectrum is that all energy levels have a huge extensive degeneracy of order $2^{N_{\rm ps}/2}$, where, in the kagome case, $N_{\rm ps}=N/3$ is the number of hexagons. The degeneracy of the spectrum has its origin in the existence of the set of operators $\tilde{\mu}(h)$, which commute with μ, and therefore with $\mathcal{H}_\mu$. The spectrum is organized in 2^{N_c} sectors labeled by the eigenvalues of the N_c independent commuting operators, which can be constructed from $\tilde{\mu}$, as explained in Sec. V E 5. The eigenvalues are identical in all the 2^{N_c} sectors. Another interesting feature is the existence of quantities that commute both with μ and with $\tilde{\mu}$, called in the following integrals of motion. They are constructed from products of μ (or alternatively $\tilde{\mu}$) on straight lines drawn on the triangular lattice of pseudospins, as explained in Appendix E. The spectrum *depends* on the values of these integrals of motion.

Using operators $\tilde{\mu}$, the dimer-dimer correlations in the model can be shown (Sec. V E 6 and Appendix D) to be short ranged.

D. One-dimensional μ-model

Before discussing the kagome case in more detail, it is interesting to look at the μ model on the one-dimensional lattice displayed in Fig. 9. As on any lattice made of corner-sharing triangles, the μ model can be defined there. The different dimer moves [and their signs $\epsilon(\alpha)$] are displayed in Fig. 14. Because it is one-dimensional, it is solvable and we will show that its spectrum exactly maps to the spectrum of the *transverse-field Ising chain at the critical field* (quantum critical point).

1. Transverse-field Ising chain

The mapping to the transverse-field Ising chain can be realized through a representation of the algebra of μ by some pseudospin operators τ^x and τ^z defined by

$$\tau^x_{2n} = \mu_{2n}, \quad \tau^x_{2n+1} = \tilde{\mu}_{2n}$$

$$\tau^z_{2n} = \prod_{l\leqslant n} \mu_{2l-1}, \quad \tau^z_{2n+1} = \prod_{l\leqslant n} \tilde{\mu}_{2l-1}. \tag{16}$$

Using the (anti)commutation relations of μ and $\tilde{\mu}$ it is easy to check that τ^x_i and τ^z_i anticommute. The μ ($\tilde{\mu}$) operators only involve the Ising pseudospins on even (odd) sites:

$$\mu_{2n} = \tau^x_{2n}, \quad \tilde{\mu}_{2n} = \tau^x_{2n+1}$$

$$\mu_{2n+1} = \tau^z_{2n}\tau^z_{2n+2}, \quad \tilde{\mu}_{2n+1} = \tau^z_{2n+1}\tau^z_{2n+3}. \tag{17}$$

And the μ Hamiltonian on the chain is now simply

$$\mathcal{H}_\mu = -\sum_n \tau^x_{2n} - \sum_n \tau^z_{2n}\tau^z_{2n+2} \tag{18}$$

which we recognize to be that of a ferromagnetic Ising chain in transverse field at its critical point.[50] This model can be solved by a Jordan-Wigner transformation (reduces to free fermions). Because the Ising chain is at its critical point, the dimer spectrum is gapless and supports linearly dispersive excitations at small momentum. In addition, $\langle \mu_i \mu_j \rangle$ correlations decay algebraically with distance. The exponential degeneracy of $\mathcal{H}_\mu$ is now transparent: only one-half of the Ising spins (located on even sites) appear to be coupled by the Hamiltonian. However, this entropy has a subtle origin: To write the μ model *only in terms of the* $N_{ps}/2$ *"coupled" degrees of freedom* (in order to get rid of the entropy) one has to use operators (τ^z_{2n}) which are nonlocal for the original dimers [see Eq. (16)]. On the other hand, there are local operators (the $\tilde{\mu}$ themselves) that do not change the energy and that create localized zero-energy excitations.

We can make a comparison with another quasi-one-dimensional model with extensive degeneracy: the spin-$\frac{1}{2}$ Heisenberg model defined on a chain of coupled tetrahedra.[51] In that model some Ising-like degrees of freedom $\chi=\pm 1$ (spin chirality) do not appear in the Hamiltonian of the low-energy sector and the model has an extensive zero-temperature entropy. This situation seems analogous to the μ model: τ^z_{2n+1} play the role of χ. However, the important difference is that τ_{2n+1} are nonlocal in terms of the original dimers, whereas χ are local in terms of the original spins.

We will see in the following sections that the μ model on the kagome lattice also has this important property that the "coupled" Ising degrees of freedom are nonlocal in terms of dimers. We are not aware of any other interacting quantum model exhibiting such kind of extensive degeneracies. There might be, however an analogy with other systems with localized excitations such as in Aharonov-Bohm cages[52] or flat-band systems in general. There, the extensive degeneracy is due to destructive interferences that prevent excitations from hopping on the lattice and thus gaining kinetic energy by delocalization. This stresses again the role of the signs in the μ operators.

2. Order parameter

The mapping to the transverse field-Ising chain suggests to introduce a different coupling for μ on odd and even sites,

$$\mathcal{H}(\Gamma) = -\Gamma \sum_n \mu_{2n} - \sum_n \mu_{2n+1} \tag{19}$$

$$= -\Gamma \sum_n \tau^x_{2n} - \sum_n \tau^z_{2n}\tau^z_{2n+2}, \tag{20}$$

so that Γ is the strength of the transverse field. It is known that the ground state has $\langle \tau^x_{2n}\rangle \neq \langle \tau^z_{2n}\tau^z_{2n+2}\rangle$ except at the critical point $\Gamma=1$. In other words, μ have different expectation values on odd and even sites for $\Gamma \neq 1$. This state ($\Gamma \neq 1$) has long-ranged $\langle \mu_i \mu_j\rangle$ correlations and is a crystal in the $\langle \mu\rangle$ variables with a diverging structure factor $S(\pi) = \Sigma_n (-1)^n \langle \mu_0 \mu_n\rangle$. It is interesting to remark that from the Ising point of view the natural order parameter is the "magnetization" $\langle \tau^z_{2n}\rangle$, which is nonzero for the $\Gamma<1$ phase but vanishes for $\Gamma \geqslant 1$. This order parameter is nonlocal in terms of the dimers [see Eq. (16)]. However, this does not mean that for $\Gamma<1$ the dimer system spontaneously breaks some hidden Ising symmetry. There is no such Ising symmetry in the dimer problem and the spurious $\mathbb{Z}_2$ redundancy was introduced in the Ising representation: reversing all τ^z gives, in fact, the *same* physical dimer state, as can be seen from Eq. (17). In the dimer language, this is a consequence of the fact that reversing all the arrows twice is proportional to the identity.

3. Heisenberg model on a frustrated ladder

The spin-$\frac{1}{2}$ Heisenberg model on the three-spin ladder shown in Fig. 9 has been studied by Waldtmann *et al.*[41] They considered a J-J' model where the horizontal coupling is J and the diagonal one (around square plaquettes) is J'. From their numerical results (exact diagonalizations for $N \leqslant 30$ spins and density matrix renormalization group (DMRG) for $N \leqslant 120$ spins) it appears that the system may be critical in the region $0.5 \lesssim J'/J \lesssim 1.25$ (vanishing spin gap) and that a spin gap opens for $J'/J \gtrsim 1.25$. Quite interestingly, they showed that at $J=J'$ the specific heat is quantitatively very similar to that of the kagome antiferromagnet and exhibits a low-temperature peak. The finite-size spectra also show a large density of singlet states above the ground state (although probably not exponential in N). These similarities suggest that the corner-sharing triangle geometry is an important ingredient to generate a large amount of low-energy singlet excitations and it would be interesting to investigate the possible relation between this three-spin ladder and the μ model.

4. Exact spectrum via fermion representation

In the mapping to the transverse field-Ising chain, we have neglected subtleties associated with boundary conditions as well as constraints on the physical space of dimer coverings. Indeed, the latter has dimension $2^{N/3+1}$ whereas we used a representation of dimension $2^{N_{\rm ps}} = 2^{N/3}$. We shall now present the full solution of the μ model on the chain, using fermionic variables.

Since we are interested mainly in the spectrum, we will realize the algebra of μ_j operators in a space that has the right dimension of the dimer space, that is, $2^{N_{\rm ps}+1}$. There exists an exact mapping between the fermionic states and the dimer states, but we do not insist on it here. We suppose periodic boundary conditions and take $N_{\rm ps}$ even.

Let us introduce a pair of creation/annihilation fermionic operators $c_j, c_j^\dagger$ at each site $j=1,\ldots,N_{\rm ps}$. They are equivalent to a pair of Majorana fermions, $\gamma_j = (c_j^\dagger + c_j)$, $\tilde{\gamma}_j = -i(c_j^\dagger - c_j)$, $\gamma_j^2 = \tilde{\gamma}_j^2 = 1$. We construct operators μ_j as follows:

$$\mu_j = i\gamma_j\gamma_{j+1}, \quad \tilde{\mu}_j = i\tilde{\gamma}_j\tilde{\gamma}_{j+1}, \tag{21}$$

so that

$$\mathcal{H}_\mu = -\sum_{j=1}^{N_{\rm ps}} \mu_j = -i\sum_{j=1}^{N_{\rm ps}} \gamma_j\gamma_{j+1}. \tag{22}$$

It is straightforward to check that two operators μ_i, μ_j anticommute if they are neighbors and commute otherwise; the same is valid for operators $\tilde{\mu}_j$, while μ_i and $\tilde{\mu}_j$ always commute.

We have not yet specified the periodicity conditions on operators γ_j. Let us introduce two extra kinetic operators, $\mu(u)$ and $\mu(d)$, which move the dimers around the two edges (or $N_{\rm ps}$-gones) of the chain

$$\mu(a) = \sum_{\alpha=1}^{2^{N_{\rm ps}-1}} \epsilon(\alpha)(|L_\alpha\rangle\langle \overline{L}_\alpha| + \text{H.c.}), \quad a=u,d$$

where α runs over $2^{N_{\rm ps}-1}$ possible loops of even length around the edge and $\epsilon(\alpha) = (-1)^{\text{Length}(\alpha)/2}$. They mutually commute and anticommute with all μ_j, $j=1,\ldots N_{\rm ps}$. Their product $\mu(u)\mu(d)$ commutes with the Hamiltonian and it is an integral of motion, taking values ± 1. Other two integrals of motion are the products of μ_j on the even (odd) sites, $\mu_o = \mu_1\mu_3\ldots\mu_{N_{\rm ps}-1}$ $(\mu_e = \mu_2\mu_4\ldots\mu_{N_{\rm ps}})$. A careful analysis shows that $\mu_o\mu_e\mu(u)\mu(d) = (-1)^{3N_{\rm ps}/2}$ on any dimer state. This constraint on physical states shows that the dimension of the Hilbert space is $2^{N_{\rm ps}+1}$. Suppose now we are in the sector with $\mu(u)\mu(d)=1$. Then, $\mu_o\mu_e = -(-1)^{N_{\rm ps}/2}\mu_1\mu_2\ldots\mu_{N_{\rm ps}}$, and using the definition from Eq. (21) we obtain that $\gamma_1\gamma_{N_{\rm ps}+1} = -1$, which implies antiperiodic boundary conditions on the Majorana fermions. In the second sector, $\mu(u)\mu(d) = -1$, the Majorana fermions have periodic boundary conditions.

We have now all that we need to solve model (22). First, all the spectrum is degenerate $2^{N_{\rm ps}/2}$ times, since all the $N_{\rm ps}$ Majorana fermions $\tilde{\gamma}_j$ commute with the Hamiltonian. Then, the Hamiltonian (22) can be diagonalized after a Fourier transformation,

$$\mathcal{H}_\mu = 2\sum_k \sin k\, \gamma_{-k}\gamma_k, \tag{23}$$

where the sum is over momenta $k = 2\pi n/N_{\rm ps}$, with n being an integer in the periodic sector a half-odd integer in the antiperiodic sector, $0 \leqslant n < N_{\rm ps}$. The operators γ_k with $0<k<\pi$ $(-\pi<k<0)$ could be interpreted as annihilation (creation) operators. Note that, in order to ensure the right com-

mutation relations between creators and annihilators, we defined the Fourier modes as $\gamma_k = 1/\sqrt{2N_{\rm ps}}\Sigma_n e^{ikn}\gamma_n$. The zero modes $k=0,\pi$ need a separate treatment, but they do not appear in the Hamiltonian. After normal ordering,

$$\mathcal{H}_\mu = 4\sum_{0<k<\pi} |\sin k|\,\gamma_{-k}\gamma_k - 2\sum_{0<k<\pi}|\sin k|. \qquad (24)$$

The vacuum energy is easily calculated in the two sectors,

$$E_0^{(-)} = -2\sum_{n=0}^{N_{\rm ps}/2-1} \sin\frac{\pi(2n+1)}{N_{\rm ps}} = -\frac{2}{\sin(\pi/N_{\rm ps})},$$

$$E_0^{(+)} = -2\sum_{n=1}^{N_{\rm ps}/2-1} \sin\frac{2\pi n}{N_{\rm ps}} = -\frac{2}{\tan(\pi/N_{\rm ps})}. \qquad (25)$$

Since $E_0^{(-)} < E_0^{(+)}$, the ground state of the dimer problem has energy $E_0 = E_0^{(-)} = -2/\sin(\pi/N_{\rm ps})$. In the thermodynamic limit $E/N_{\rm ps} \to -2/\pi$. The first-excited state is at $E_0^{(+)}$; the rest of the spectrum can be constructed by making particle-hole excitations over the two fermionic vacua, according to Eq. (24). The numerical spectra, obtained in the dimer representation, are in complete agreement with those constructed from Eq. (24). In the thermodynamic limit, the gap vanishes and the excitation spectrum of γ_k is linear at small momentum.

E. Kagome case

1. Degenerate representation

As we did in the one-dimensional case, it is natural to represent the μ operators with Ising variables. The simplest representation uses one Ising variable $\tau^z = \pm 1$ at each hexagon:

$$\mu_{\mathbf{r}} = \tau^x_{\mathbf{r}}\prod_{i=1}^{3}\tau^z_{\mathbf{r}+\mathbf{e}_i}, \quad \tilde{\mu}_{\mathbf{r}} = \tau^x_{\mathbf{r}}\prod_{i=1}^{3}\tau^z_{\mathbf{r}-\mathbf{e}_i}, \qquad (26)$$

where the three unit vectors $\mathbf{e}_i$ are at 120 deg and relate a site to three of its neighbors on the triangular lattice. It is easy to check that this representation indeed realizes the μ (and $\tilde{\mu}$) algebra. One can, in fact, express μ in terms of ZE pseudospin operators σ^z and find similar (although more complicated) relations (see Appendix B). Notice, in particular, that τ^z anticommutes with μ and $\tilde{\mu}$ on the same hexagon but commutes with all the others, exactly as σ^z do. This representation has (approximately) the correct size of the Hilbert space ($\sim 2^{N_{\rm ps}}$), but it does not show how many Ising variables decouple in this model, that is how large is, the degeneracy (entropy) in this model.

2. Three-sublattice representation

One can use a different representation for the μ's on a smaller subspace, therefore removing part of the degeneracy. Consider a decomposition of the triangular lattice into *three* sublattices A,B, and C. All the $\tilde{\mu}(c)$ with $c \in C$ commute with each other (as well as with all the μ). They can be simultaneously diagonalized so that we can consider an eigenstate $|\psi_0\rangle$ of these $\tilde{\mu}(c)$:

$$\tilde{\mu}(c)|\psi_0\rangle = \eta(c)|\psi_0\rangle, \quad \eta(c) = \pm 1. \qquad (27)$$

In addition, we may define some operators $s(h)$ by

$$s(h) = \mu(h)\tilde{\mu}(h). \qquad (28)$$

They are diagonal in the dimer basis and commute with each other. We can project $|\psi_0\rangle$ onto the subspace, where $s(c) = \eta(c)$ for any site $c \in C$:

$$|\psi_1\rangle = \prod_{c\in C}\left(\frac{1+\eta(c)s(c)}{2}\right)|\psi_0\rangle, \qquad (29)$$

which, by Eq. (27), is simply

$$|\psi_1\rangle = \prod_{c\in C}\left(\frac{1+\mu(c)}{2}\right)|\psi_0\rangle. \qquad (30)$$

Now we consider the states generated by the action of $\mu(a\in A)$ and $\mu(b\in B)$ on $|\psi_1\rangle$. A basis can be labeled by $2N_{\rm ps}/3$ Ising variables $\tau^z_a = \pm 1$ and $\tau^z_b = \pm 1$ as follows:

$$|\tau^z_a, \tau^z_b\rangle = \left[\prod_{a\in A}\mu(a)^{1/2(1+\tau^z_a)}\right]\left[\prod_{b\in B}\mu(b)^{1/2(1+\tau^z_b)}\right]|\psi_1\rangle. \qquad (31)$$

As we will now show, this subspace is stable under the action of any μ. This is obvious concerning the operators μ located on sublattices A and B. On these sites we may define (nondiagonal) τ^x operators which reverse the value of τ^z at the corresponding site. With this definition, we have

$$\mu(a) = \tau^x_a, \qquad (32)$$

$$\mu(b) = \tau^x_b\tau^z_a\tau^z_{a'}\tau^z_{a''}. \qquad (33)$$

The $\tau^z_a\tau^z_{a'}\tau^z_{a''}$ comes from the anticommutation of $\mu(b)$ with its three neighbors (a, a', and a'') belonging to A when acting on a state such as Eq. (31). Now we act with a $\mu(c)$ on $|\tau^z_a, \tau^z_b\rangle$. Upon moving $\mu(c)$ to the right through $\mu(a)$ and $\mu(b)$, the state picks a sign $\tau^z_a\tau^z_{a'}\tau^z_{a''}\tau^z_b\tau^z_{b'}\tau^z_{b''}$ where $a,a',\ldots,b''$ are the six neighbors of c. Then we use the fact that $\mu(c)|\psi_1\rangle = |\psi_1\rangle$ so that we finally get the following representation:

$$\mu(a) = \tau^x_a,$$

$$\mu(b) = \tau^x_b\tau^z_a\tau^z_{a'}\tau^z_{a''},$$

$$\mu(c) = \tau^z_a\tau^z_{a'}\tau^z_{a''}\tau^z_b\tau^z_{b'}\tau^z_{b''}. \qquad (34)$$

This representation is independent of $\eta(c)$. As a consequence, the spectrum of any Hamiltonian made out of μ operators (such as $\mathcal{H}_\mu$) will be at least $2^{N_{\rm ps}/3}$-fold degenerate. As we show later, this degeneracy is, in fact, much larger $\sim 2^{N_{\rm ps}/2}$ but this already exhibits an extensive residual entropy at zero temperature.

3. Mean-field approximation

The representation of Eq. (34) suggests a simple variational (or mean-field) approximation in which the system is in a tensor product of single-site wavefunctions $|\Psi\rangle = \otimes_1^{N_{ps}/3}(|\Psi_A\rangle \otimes |\Psi_B\rangle)$. All the sites $a \in A$ are in the same state as well as all the $b \in B$:

$$|\Psi_A\rangle = \cos(\theta/2)|\uparrow\rangle + \sin(\theta/2)|\downarrow\rangle, \tag{35}$$

$$|\Psi_B\rangle = \cos(\phi/2)|\uparrow\rangle + \sin(\phi/2)|\downarrow\rangle. \tag{36}$$

We have two variational parameters θ and ϕ and the expectation value of the energy per hexagon is

$$\langle \mu_a \rangle = \sin(\theta),$$

$$\langle \mu_b \rangle = \cos(\theta)^3 \sin(\phi), \tag{37}$$

$$\langle \mu_c \rangle = \cos(\theta)^3 \cos(\phi)^3,$$

$$E/N_{ps} = -\tfrac{1}{3}(\langle \mu_a \rangle + \langle \mu_b \rangle + \langle \mu_c \rangle). \tag{38}$$

Minimizing E we get

$$\langle \mu_a \rangle \simeq 0.2979; \ \langle \mu_b \rangle \simeq 0.3104; \ \langle \mu_c \rangle \simeq 0.7091 \tag{39}$$

$$E/N_{ps} = -0.4391. \tag{40}$$

Because $\langle \mu_a \rangle \neq \langle \mu_b \rangle \neq \langle \mu_c \rangle$, this state breaks the translation symmetry. It has some crystalline order with respect to the $\langle \mu \rangle$ variables. Notice, however, that such a state is *not a dimer crystal* [see Eq. (D9)], since it can be chosen to have zero dimer-dimer correlations beyond a few lattice spacings. From the numerical diagonalizations, we estimate the exact ground-state energy to be $E/N_{ps} \simeq -0.44 \pm 0.02$ (see Sec. VI and Fig. 18), which agrees with the variational result within error bars. It is interesting to compare these energies with the energy that one gets with a single-site wave function derived from the translation invariant representation of Eq. (26). The later approximation gives $E/N_{ps} = -0.3248$, which is significantly higher. Two other mean-field states can be considered from Eq. (26). On can use three different single-spin states $|\Psi_A\rangle$, $|\Psi_B\rangle$, and $|\Psi_C\rangle$ on three sublattices. Minimizing energy with respect to the three related angles we get $E/N_{ps} = -1/3$. The corresponding variational state simply has $\langle \mu_a \rangle = 1$, $\langle \mu_b \rangle = \langle \mu_c \rangle = 0$. Enlarging the unit cell does not help to lower energy. Indeed, using four sublattices leads to an even worse energy ($E/N_{ps} = -1/4$, $\langle \mu_a \rangle = 1$ and $\langle \mu_{b,c,d} \rangle = 0$). The fact that the degenerate representation gives rather bad energies can be explained from the fact that in such states the Ising degrees of freedom (τ^x or τ^z) are completely uncorrelated on different sites: $\langle \tau_i \tau_j \rangle = \langle \tau_i \rangle \langle \tau_j \rangle$. The situation is different in a representation such as Eq. (34). In that case nontrivial nearest-neighbor correlations are present even in simple tensor-product states such as the one we considered.

Although the good variational energy given in Eq. (40) does not prove that the system indeed spontaneously breaks the translation symmetry, it indicates that the μ model on the kagome lattice is not very far from such a phase.[53] The numerical results presented in Sec. VI indeed show that, at least at short distances, $\langle \mu(x)\mu(y) \rangle$ correlations match the three-sublattice pattern.

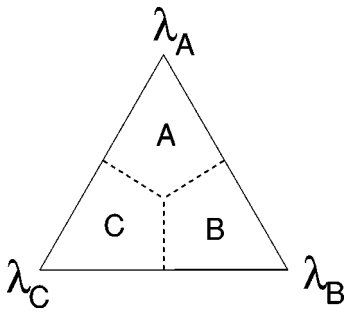

FIG. 15. Mean-field phase diagram of the μ model on the kagome lattice with three different couplings λ_A, λ_B, and λ_C on three sublattices. Because the mean-field approximation breaks the symmetry which exchanges *A*, *B* and *C*, the transition lines (dashed) do not precisely match the symmetry axis. Such symmetry should hold in the real system and was restored here for clarity. Transitions are first order.

4. Three-sublattice μ model

As for the one-dimensional model, we can generalize the kagome μ model by letting the couplings be different on sublattices *A*, *B*, and *C*:

$$\mathcal{H} = -\lambda_A \sum_{a \in A} \mu_a - \lambda_B \sum_{b \in B} \mu_b - \lambda_C \sum_{c \in C} \mu_c \tag{41}$$

and we focus on $\lambda_A + \lambda_B + \lambda_C = 1$ and $\lambda_A, \lambda_B, \lambda_C \geqslant 0$. We determined the ground state of the model within the mean-field approximation of Eqs. (37) and (38). The result is schematically shown in Fig. 15 (a qualitatively similar phase diagram is obtained with the degenerate representation). We obtain three phases. When λ_A dominates, the ground state has $\theta = \pi/2$, $\langle \tau_a^z \rangle = 0$, and $\langle \tau_b^z \rangle \neq 0$. When λ_B is the strongest, we have $\phi = \pi/2$, $\langle \tau_a^z \rangle \neq 0$, and $\langle \tau_b^z \rangle = 0$. Close to the λ_C point, we have $\langle \tau_a^z \rangle \neq 0$ and $\langle \tau_b^z \rangle \neq 0$. Along the transition lines (dashed line in Fig. 15) an expectation value $\langle \tau^z \rangle$ jumps from zero to a finite value so that the transitions are first order in this approximation.

The mean-field prediction for the topology of the phase diagram appears to be quite plausible. If there are indeed three phases, then, by symmetry, the point of interest $\lambda_A = \lambda_B = \lambda_C$ is the end point of three transition lines. It is not clear whether the discontinuous character of these transitions is an artifact of the mean-field approximation or a robust property. If the transitions are really first order, then the μ model spontaneously breaks the translation invariance and realizes a crystal in the μ variables. It may also be that $\lambda_A = \lambda_B = \lambda_C$ is a critical point. Although we have no definite conclusion on this issue, some of the numerical results (susceptibility) presented in Sec. VI suggest a critical point.

5. Nondegenerate representation

The constructions above use at most $N_{ps}/3$ commuting $\tilde{\mu}$ operators, but this is not the maximum number N_c of mutu-

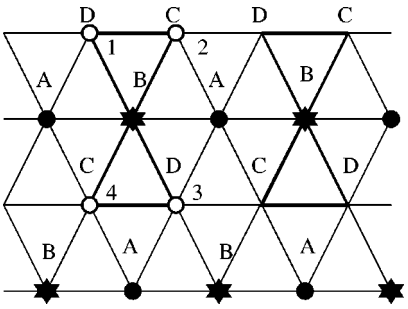

FIG. 16. Dividing the triangular lattice in four sublattices *A*, *B*, *C*, and *D*. The open dots represent the spins entering a bow-tie operator centered on the *B* sublattice. The black dots and the stars correspond to the positions of spins and centers of the bow-tie operators, respectively, forming a set of mutually commuting operators.

ally commuting operators made out of $\tilde{\mu}$. In fact, there are of the order of $N_c \simeq N_{\rm ps}/2$ Ising degrees of freedom that decouple, as can be seen from the following argument. Divide the lattice in *four* sublattices A,B,C,D as shown in Fig. 16. The "spins" $\tilde{\mu}(h)$ on the *A* sublattice mutually commute. In addition, one can consider the "bow-tie" operators $\tilde{T} = \tilde{\mu}(1)\tilde{\mu}(2)\tilde{\mu}(3)\tilde{\mu}(4)$, centered on sites of the *B* sublattice and involving neighboring "spins"of the *C* and *D* sublattices. These $N_{\rm ps}/4$ bow-tie operators commute mutually and with the operators $\tilde{\mu}(h)$ from the *A* sublattice, which gives us an ensemble of $N_{\rm ps}/2$ commuting operators.[54] These conserved quantities ($\tilde{\mu}$ and $\tilde{T}$) can be used to eliminate degrees of freedom on the two sublattices in a similar way as we did for the three-sublattice representation. However, now, one cannot avoid obtaining a nonlocal representation of the μ algebra in terms of the spins living on the *C* and *D* sublattices. The procedure is briefly explained in Appendix. C.

6. Arrow and dimer correlations

Using the $\tilde{\mu}$ and $\tilde{T}$ introduced above, it is possible to demonstrate (see Appendix D) that dimer-dimer correlations vanish identically beyond a few lattice spacings in any state that is an eigenstate of all the $\tilde{\mu}(a \in A)$ and $\tilde{T}(b \in B)$. Since the eigenstates of the Hamiltonian can be choosen to be eigenstates of these $\tilde{\mu}(a \in A)$ and $\tilde{T}(b \in B)$, one can choose a basis of the ground-state manifold where every state is a *dimer liquid*. The same result was found in Ref. 21 in a gapped dimer model. Here, because the ground state manifold has a huge dimension, it is likely that some perturbations are able to select (out of the ground state manifold of $\mathcal{H}_\mu$) states with some dimer order. Even in such a case we expect dimer-dimer correlations to be very weak in the vicinity of $\mathcal{H}_\mu$.

7. Fermionic representation

A version of the arrow representation can be given in terms of fermions. The advantage of such a formulation is that signs are naturally included. Unlike the one-dimensional case, such a fermionic representation cannot be used anymore to solve the model, since the Hamiltonian (15) cannot be reduced to a quadratic form in fermions. However, it is still useful in gaining some insight about the model, for example, it helps in understanding the extensive degeneracy of the spectrum. In particular, it provides an argument that shows that the degeneracy is $\sim 2^{N_{\rm ps}/2}$ *not only on the kagome lattice but also on any lattice made of corner-sharing triangles provided the lattice of triangles* (lattice *H* of Sec. III A) is *bipartite*.

We associate to each vertex of the kagome lattice a fermionic occupation number 0 or 1. For a given dimer configuration, the corresponding fermion configuration is given by the following rules: a defect triangle has either occupation numbers 111 or 000. In other triangles, there is one dimer connecting the sites with equal fermion numbers, 00 or 11. There is a constraint on the parity of the number of fermions on each triangle, alternating on adjacent triangles, for example, triangles pointing to the right in Fig. 5 have odd numbers of fermions, and those pointing to the left have even number of fermions. It is not difficult to see that the arrow variables and the occupation number variables are essentially the same and that their constraints are of the same nature. In particular, the counting of the degrees of freedom is similar for arrows and fermions, the constraint for each triangle eliminating one spurious degrees of freedom.

On each kagome site there is a pair of creation/annihilation fermionic operators $c_j, c_j^\dagger$. As explained above, the dimer space is equivalent to the fermion Fock space, with constraints on the occupation number on each triangle. As in the case of the chain, we transform the fermions into a pair of Majorana fermions, $\gamma_j = (c_j^\dagger + c_j)$, $\tilde{\gamma}_j = -i(c_j^\dagger - c_j)$. The algebra of operators $\mu(h)$ can be realized now by using only operators γ_j,

$$\mu(h) = i \overrightarrow{\prod_j} \gamma_j$$

where the arrow means that the product is oriented (for example, it starts at the leftmost site of the hexagon and runs clockwise). With this representation the μ model contains six fermionic creation or annihilation operators. Since two adjacent hexagons have one kagome site in common, the associated μ operators anticommute. Distant μ's commute, since they are constructed from an even number of fermions, and each operators μ squares to 1. Similarly, one can construct

$$\tilde{\mu}(h) = -i \overleftarrow{\prod_j} \tilde{\gamma}_j,$$

with the product running in the opposite direction to that of μ. These operators obey the same algebra as $\mu(h)$ and commute with the whole set of operators μ. The symmetric role played by operators γ_j and $\tilde{\gamma}_j$ suggests that one-half of the degrees of freedom are not affected by the action of the Hamiltonian Eq. (15) and, therefore, that the degeneracy of the spectrum is of the order of $2^{N_{\rm ps}/2}$.

Let us note that operators $\mu(h)$ and $\tilde{\mu}(h)$ leave the constraints on the occupation numbers invariant, since they

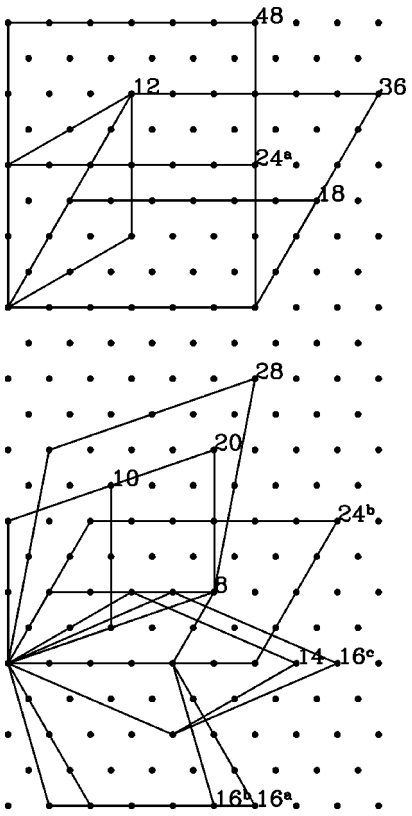

FIG. 17. Finite-size lattices used for the numerical diagonalizations of the μ model. Each dot is a hexagon of the kagome lattice. $N_{\rm ps}=\frac{1}{3}N$ is indicated. The lattices on the top are compatible with a three-sublattice structure whereas the others (bottom) are not. All lattices except $N_{\rm ps}=10,14,16^b,16^c$ are compatible with the four-sublattice structure.

change by 2 the occupation number on each triangle. More generally, products of γ on loops that visit each triangle an even number of times also leave the constraints invariant and their action could be translated in the dimer language. The most general operator that preserves the constraint (dimer space) can be constructed from the products of γ and $\tilde{\gamma}$ on loops visiting each triangle an even number of times. These operators are the equivalent of Wilson loops in a gauge theory. Triangles where the constraint is not obeyed can be constructed by the action of strings of γ operators (they could be useful for describing dimer configurations with defects, and therefore to introduce holons or spinons). And finally, the vison creation operator is naturally constructed in this language as the product of $\gamma_i\tilde{\gamma}_i$ on a string.

The fermionic representation allows one to study the integrals of motion and to prove that they are associated with the closed straight lines on the lattice. In Appendix E, these integrals of motion are constructed, and used to build a complete set of quantum numbers for the dimer Hilbert space.

VI. EXACT DIAGONALIZATIONS OF THE μ-MODEL

Because the nondiagonal matrix elements of the μ operator have different signs, $\mathcal{H}_\mu$ is not appropriate for large-scale Monte Carlo simulations and, instead, we performed some

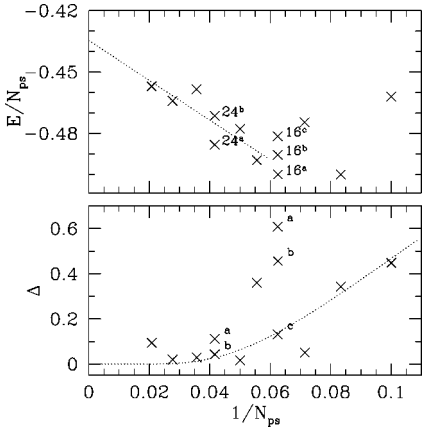

FIG. 18. Top: Ground-state energy per site. The dotted line is a least-square fit of the data for $N_{\rm ps}>16$. Bottom: energy gap between the ground-state multiplet and the first-excited state. The dotted line is a guide to the eye ($\sim e^{-aN_{\rm ps}}$). When different values are plotted for the same $N_{\rm ps}$, they correspond to different shapes (see $N_{\rm ps}=16$ and 24 in Fig. 17).

numerical diagonalizations of the Hamiltonian. For systems up to $N_{\rm hex}=N_{ps}=16$ hexagons ($N=48$ sites) we diagonalize it directly in the basis of dimer coverings (whose dimension is $2^{N_{\rm ps}+1}$) by using all lattice symmetries. For larger systems ($N_{\rm ps}=20$, 24, 28, 36) we diagonalize the Hamiltonian in a representation where the extensive degeneracy (due to the N_c Ising quantities that commute with every μ_i) have been removed (see Appendix C). The diagonalization is performed separately for each sector defined by the conserved quantities *I*. For the largest system ($N_{\rm ps}=48$, $N=144$) we use a Lanczos algorithm in this nondegenerate representation to obtain the first energies and wave functions. Thanks to these numerous symmetries the largest vector size is only $\sim 10^6$. The lattices we used are displayed in Fig. 17.

A. Spectrum

The ground state energy per hexagon is plotted in Fig. 18. From this data we can estimate that $\langle\mu\rangle\simeq -0.44\pm 0.02$ in the thermodynamic limit. It is interesting to compare this value with the energy of a simple 4-μ problem $\mathcal{H}=\mu_1+\mu_2+\mu_3+\mu_4$ (with periodic boundary condition so that every site is neighbor of the three others), which has $\langle\mu\rangle=-\frac{1}{2}$ in its ground state.[55] The energy gap between the ground state multiplet and the first-excited state is also shown in Fig. 18. This quantity probably goes to zero in the thermodynamic limit. Figure 19 shows the gap as a function of the ground state energy per hexagon. It appears that the samples with the largest gap are those whose energy is significantly lower than the thermodynamic estimate ($\langle\mu\rangle\simeq -0.44\pm 0.02$). This also points to a gapless spectrum in the limit of large systems.

The dispersion relation of the first-excited states usually provides some useful insight. However, due to the extensive degeneracy, this brings no information for the μ model because the dispersion relation can be shown to be perfectly flat. Let $|k\rangle$ be an eigenstate with momentum k and energy

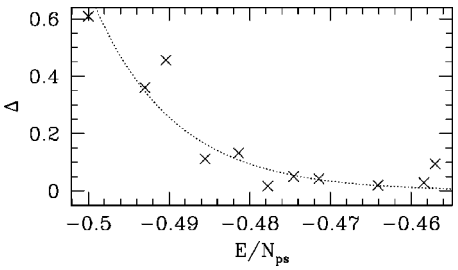

FIG. 19. Gap as a function the energy per site for $N_{\rm ps}>12$ (data of Fig. 18). The line is a guide to the eye.

E_k. The new state $|k+q\rangle=\Sigma_h e^{i\mathbf{q}\cdot\mathbf{r}_h}\tilde{\mu}(h)|k\rangle$ has, by construction, momentum $k+q$. Because $\tilde{\mu}$ commute with $\mathcal{H}_\mu$, $|k+q\rangle$ is still an eigenstate with energy E_k. This property is just a consequence of the fact that acting with a $\tilde{\mu}$ creates a *localized* zero-energy excitations.

From these data we propose two possible scenarios.

(1) An additional ground-state degeneracy associated with some spontaneous symmetry breaking in the thermodynamic limit. As we will explain, it may be that the ground state orders in the three-sublattice pattern discussed in Sec. V E 3. As we will explain, this scenario does not seem to be the most likely. In particular, if the system was a three-sublattice crystal in the μ variables, the spectrum would have a ground state with a small[56] quasidegeneracy (ignoring the exponential factor coming from the $\tilde{\mu}$ degrees of freedom) separated by a *gap* to higher excitations. This does not seem to be the case since we could not identify a small set of energy levels adjacent to the ground state above which a significant gap could exist.

(2) In the second scenario, the low-energy states may correspond to a gapless mode of excitations in the system. Although we have no precise theoretical prediction for the nature of such (critical) excitations in this two-dimensional dimer model, gapless excitations are reminiscent of the one-dimensional analog (which has fermionic critical excitations at low energy, see Sec. V D concerning the μ model on the chain). According to the single-mode approximation discussed in Sec. VI D these gapless excitations would only exist at a finite value of momentum.

B. Correlations

We looked for the possibility of long-ranged $\mu_i\mu_j$ correlations in the ground state. We define a static structure factor $S(k)$ in the usual way:

$$S(k)=\frac{1}{N_{\rm ps}}\langle 0|\mu_k\mu_{-k}|0\rangle \tag{42}$$

$$=\frac{1}{N_{\rm ps}}\sum_{i,j} e^{-ik\cdot(r_i-r_j)}\langle 0|\mu_i\mu_j|0\rangle, \tag{43}$$

where

$$\mu_k=\sum_i e^{-ik\cdot r_i}\mu_i . \tag{44}$$

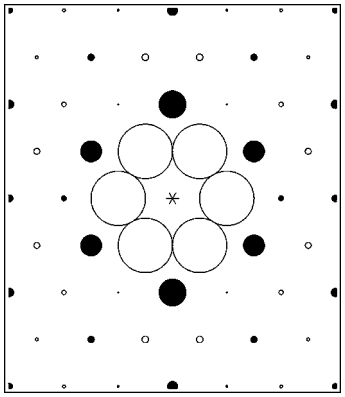

FIG. 20. Correlations $\langle\mu_0\mu_i\rangle^c=\langle\mu_0\mu_i\rangle-\langle\mu_0\rangle^2$ in a 48-hexagon system. The site 0 is at the center. The radius of the circles is proportional to $|\langle\mu_0\mu_i\rangle^c|$. Empty circles indicate negative correlations and the black ones are for $\langle\mu_0\mu_i\rangle^c\geqslant 0$

These calculations were done numerically in a reduced Hilbert space where $N_c\sim N_{\rm ps}/2$ conserved quantities (made out of $\tilde{\mu}$ and $\tilde{T}$ operators) are fixed to be ± 1 (nondegenerate representation). By construction the spectrum does not depend on these choices (that is, the origin of the entropy) but it is also possible to check that $\langle\mu_i\mu_j\rangle$ correlations do not depend either on the sector. However, we stress that it is, in principle, possible to have different correlations in a ground state, which would be a linear combination of the ground states of different sectors. This is similar to the question of dimer-dimer correlations discussed previously. We have not investigated these effects which are related to the possible ordering pattern, which may be selected by small perturbations in the ground state manifold.

The results are summarized in Figs. 20–22. Figure 21 clearly indicates that the most important correlations appear at the border of the Brillouin zone. More precisely the corners of the Brillouin zone $k_B=(\pm 4\pi/3,0)$ and the middle points of the borders of the Brillouin zone $k_{A_1}=(0,2\pi/\sqrt{3})$, $k_{A_2}=(\pi,-\pi/\sqrt{3})$, and $k_{A_3}=(\pi,\pi/\sqrt{3})$ are

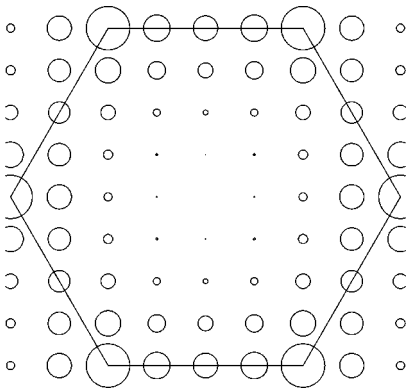

FIG. 21. Structure factor $S(k)=1/N\langle\mu_{-k}\mu_k\rangle$ represented in the first Brillouin zone of the triangular lattice for $N_{\rm ps}=48$ (144 kagome sites). The radius of the circle is proportional to $S(k)$. $S(k)$ has a trivial divergence at $k=0$ which is due to the fact that operator $\langle\mu_i\rangle$ is nonzero at every site. This peak at $k=0$ is not represented here.

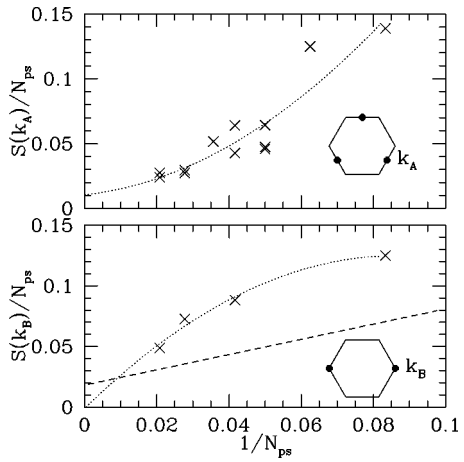

FIG. 22. Top: structure factor at $k=k_A$. Bottom: Structure factor at $k=k_B$. The dotted lines are obtained by a least-square fit of the form $a+bN_{\mathrm{ps}}^{-1}+cN_{\mathrm{ps}}^{-2}$. The dashed line is the mean-field [Eq. (40)] prediction for $S(k_B)/N_{\mathrm{ps}}$. The quick reduction of the crystal order parameter with the system size (compared with the mean-field result) suggests that the crystal is unstable to fluctuations. The analysis of the related susceptibilities confirms that $S(k)/N_{\mathrm{ps}}$ is indeed likely to extrapolate to zero when $N_{\mathrm{ps}}\rightarrow\infty$.

the reciprocal lattice points where the correlations are the strongest. k_B correspond to a three-sublattice structure whereas k_{A_i} is related to a two-sublattice (stripelike) order. A (weak) tendency to a three-sublattice ordering can been seen directly in Fig. 20, which represents real-space correlations in the ground state of the $N_{\mathrm{ps}}=48$ sample (144 kagome sites). Almost all the sites with a positive correlation (black circles) are located on the same sublattice (according to a three-sublattice decomposition) as the reference site.

To check whether these correlations could remain long ranged in the thermodynamic limit we plot $S(k)/N_{\mathrm{ps}}$ as a function of N_{ps} (see Fig. 22). As a result, $S(k)/N_{\mathrm{ps}}$ seems to extrapolate to a very small (possibly 0) value in the limit of large systems. This suggests neither two- nor three- sublattice ''crystalline'' order in the expectation values of the μ operators. However, the data at $k=k_B$ should be compared with the mean-field state described in Sec. V E 3. According to the expectation values given by Eq. (39) we should have $S(k)/N_{\mathrm{ps}}\simeq 0.0182$ in the thermodynamic limit. While the extrapolation of the numerical results of Fig. 22 cannot distinguish such a small-order parameter from a disordered (or critical) phase, the prediction of the mean-field approximation (dashed line in Fig. 22) turns out to be significantly different from the exact ones. In the mean-field approximation $S(k_B)$ is given by $S(k_B)/N_{\mathrm{ps}}\simeq 0.0182+0.6279/N_{\mathrm{ps}}$ (the $1/N_{\mathrm{ps}}$ contribution is just the local contribution of a given site and its six neighbors). On the other hand, the exact value of $S(k_B)/N_{\mathrm{ps}}$ decays much faster with N_{ps}. This means that the reduction of the crystal order parameter $S(k_B)/N_{\mathrm{ps}}$ with the system size is mainly caused by long-wave length fluctuations rather than by local contributions. This is a serious indication that the three-sublattice crystal is unstable with respect to these fluctuations.

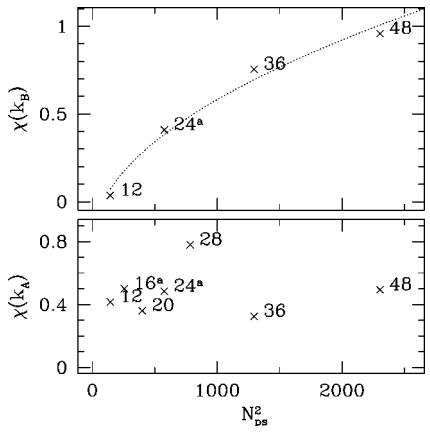

FIG. 23. Static susceptibility $\chi(k)$ for the wave vectors ($k=k_A$ and $k=k_B$) where correlations are the strongest. Long-range order with spontaneous symmetry breaking would imply $\chi\sim N^2$, which does not appear to be satisfied. The dotted line is a least-square fit of the form $\chi(k_B)\simeq aN+b$.

C. Static susceptibility

To get more insight into the possibility of some crystalline order in the μ variables we calculated the static susceptibilities $\chi(k)$:

$$\chi(k)=\frac{1}{2N_{\mathrm{ps}}}\frac{\partial\langle\mu_k+\mu_{-k}\rangle}{\partial\lambda}, \tag{45}$$

where λ is the strength of an infinitesimal symmetry-breaking perturbation,

$$\mathcal{H}_\lambda=\sum_i \mu_i-\frac{1}{2}\lambda(\mu_k+\mu_{-k}) \tag{46}$$

$\chi(k)$ is obtained numerically by measuring the expectation value of $\mu_k+\mu_{-k}$ in the ground state of the Hamiltonian Eq. (46) in the presence of a small perturbation. The susceptibility is obtained by extrapolating the result to $\lambda=0$.

The static susceptibility is a rather sensitive probe since it must diverge as N_{ps}^2 in systems that spontaneously break the translation symmetry in the thermodynamic limit.[57] On the other hand, it remains finite if there is no ordering at the corresponding wave vector. The results for $k=k_A$ and $k=k_B$ are displayed in Fig. 23. $\chi(k)$ shows no tendency to diverge at $k=k_A$ and the increase with N_{ps} of $\chi(k_B)$ is significantly slower than $\sim N_{\mathrm{ps}}^2$, as suggested by the rather good fit obtained with $\chi(k_B)\simeq aN_{\mathrm{ps}}+b$ (dotted line in Fig. 23). For these reasons we think that the system does not develop long-ranged $\mu_i\mu_j$ correlations in the thermodynamic limit. The data for $\chi(k_B)$ (which neither diverges like N_{ps}^2 nor stays constant) might be interpreted as a proximity to a *critical point* where a three-sublattice structure would appear.

D. Long-wavelength fluctuations

We now turn to the analysis of the long-wavelength fluctuations in the system. The structure factor $S(k)$ is represented as a function of $|k|$ in Fig. 24. $S(k)$ seems to vanish at least as $S(q)\sim|k|^2$ and probably faster. A $\sim|k|^4$ behavior

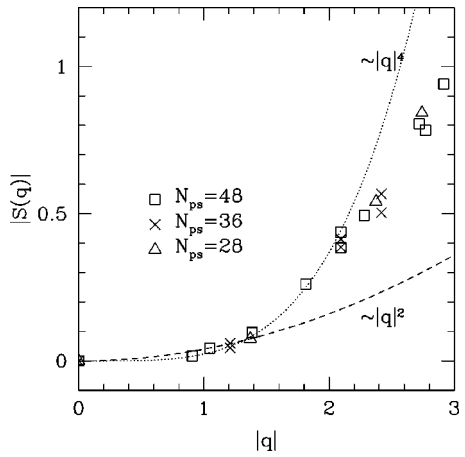

FIG. 24. Long-wavelength behavior of the structure factor $S(k)$ for different sample sizes.

looks plausible and is reminiscent of quantum Hall effect.[58] As explained before, the dispersion relation is flat in this model. However, one may be interested in the excitations that can be created by the action of the μ operators *only* (excluding $\tilde{\mu}$). Such a variational excited state with momentum k can be constructed from the ground state in the spirit of the single-mode approximation:

$$|k\rangle = \mu_k|0\rangle. \tag{47}$$

The energy (relative to the ground-state) of $|k\rangle$ is

$$\omega(k) = \frac{\frac{1}{2N_{\rm ps}}[\mu_{-k},[\mathcal{H},\mu_k]]}{S(k)}. \tag{48}$$

Since the numerator (oscillator strength) behaves, as usual, as $\sim|k^2|$ at small $|k|$, we find that $|k\rangle$ is not a low-energy excitation as soon as $S(k)$ vanishes like $|k|^2$ or faster—which seems to be the case. This is suggestive of a nonzero gap for zero-momentum excitations.

VII. DISCUSSION AND CONCLUSIONS

We have introduced a QDM on the kagome lattice with a kinetic energy that allows from three to six dimers to resonate around hexagons. The crucial difference with previous QDM is that dimers move with amplitudes that have nontrivial signs inherited from the underlying spin-$\frac{1}{2}$ model. Exploiting the algebraic properties of the conserved quantities ($\tilde{\mu}$ operators), we showed that the model has an extensive entropy at zero temperature—$\frac{1}{6}\ln(2)$ per kagome site—and is a dimer liquid.

The starting point of this study was the spin-$\frac{1}{2}$ Heisenberg model on the kagome lattice. Concerning this problem, our main result is that a high density of singlet states at low energy might have a real quantum origin and may not just be the remainder of the local degeneracies of the classical model. The mechanism that produces the entropy of the μ model requires one to use nonlocal degrees of freedom in order to compute the spectrum in a representation that eliminates the degeneracy. We are not aware of any other model with a similar behavior. Going from the KAFH model to the μ model we made some crude approximations. The first one was to reduce the spin Hilbert space to a short-range RVB one. We provided several arguments to support this approximation but some additional studies would be required to analyze this question further. The second drastic approximation was to reduce the dimer dynamics induced by the Heisenberg interaction to that of the μ model and its *signs*. This can be qualitatively justified for the KAFH in the temperature regime corresponding to the low-temperature peak of the specific heat. If that picture is correct, the degrees of freedom involved in that peak would correspond to the $\sim N_{\rm ps}/2 = N/6$ uncoupled degrees of freedom of the μ model. The μ model can be defined on any lattice made of corner-sharing triangles, it could, therefore, provide a rather general explanation for a large entropy at low temperature in the corresponding frustrated spin-$\frac{1}{2}$ models. Determining if some order eventually develops at much lower temperatures would amount to analyze a degenerate perturbation theory in the ground state manifold of the μ model.

An important question is to know whether the μ model realizes a new phase or if it is at a critical point. We have shown that the most serious candidate for an ordered phase, if any, is the three-sublattice crystal. However, we gave several indications (spectrum, correlations, and susceptibility) suggesting that it is not stable. Instead we suggest that the system might be at a critical point. If we think of a dimer model as a system of hard-core bosons, it is interesting to compare our findings with some known bosonic phases. Let us first come back to the gapped RVB state realized in the solvable QDM of Ref. 21. That state, which is the equal-amplitude superposition of all dimer configurations (Rokhsar-Kivelson[18] state), is very similar to a Bose-Einstein *condensate* in the sense that its wave function can be obtained by putting all dimers in the same zero-momentum state.[59] The important difference from a conventional superfluid is that the dimer model has no U(1) gauge symmetry (and therefore no gapless ''sound'' mode or conserved integer charge) but a discrete $\mathbb{Z}_2$ gauge symmetry.[21] With that comparison in mind, the ground state of the μ model would neither be a condensate nor a crystal but it has *gapless* excitations. This is rather unusual in a model that has no continuous symmetry at all. In addition, our model has a structure factor $S(q)$ for $\langle\mu\mu\rangle$ correlations, which decays as $|q|^2$ or faster in the limit $q\to 0$. In a single-mode approximation this would imply a gap for $q=0$ excitations.

In order to study the spectrum of the μ model we used a representation in which the degrees of freedom responsible for the extensive entropy are frozen. The μ model is local in the dimer variables but the effective Hamiltonian describing the nondegenerate spectrum turned out to be nonlocal in terms of the original dimers. These effective long-ranged interactions between physical degrees of freedom might be an important ingredient for the appearance of an exotic liquid. From this point of view, there might be some similarities between the μ model and some two-dimensional quantum systems of Bosons with long-ranged interactions. Exotic liquid states, which are not superfluid, have been proposed for

these systems, including a quantum hexatic phase.[60,61] On the other, hand a critical Bose fluid can exist without long range interactions and such a phase can be stabilized by cyclic ring-exchanges.[62,63] A striking feature of these new phases is the existence of gapless excitations along *lines* in the Brillouin zone, as in a Fermi liquid. We have no direct indication of such a behavior in the kagome μ model, except for the existence of a fermionic representation, but such a scenario is certainly an interesting possibility that should be tested in future studies.

ACKNOWLEDGMENTS

We are grateful to C. Lhuillier, F. Mila, R. Moessner, and M. Oshikawa for several fruitful discussions. Numerical diagonalizations of QDM models were done on the Compaq alpha server of the CEA under Project No. 550.

APPENDIX A: ZENG AND ELSER'S PSEUDOSPINS REPRESENTATION OF DIMER COVERINGS

Zeng and Elser (ZE) realized[5,6] that a close correspondence between Ising configurations of pseudospins sitting on hexagons and dimer configurations on the kagome lattice (within a given topological sector) could be used. We used this representation in a previous work[21] to define an exactly solvable quantum dimer model. In this section we review the pseudospin representation.

1. σ^z component

We first need an (arbitrary) reference dimer configuration $|D_0\rangle$. We will associate a pair of pseudospin configurations $\{\sigma_h^z=\pm 1\}_{h\in \text{hex.}}$ with any dimer configuration $|D\rangle$ (belonging to the topological sector of $|D_0\rangle$) in the following way.

(1) Draw the loops of the transition graph of $\langle D_0|D\rangle$.

(2) These loops must be considered as domain walls separating hexagons where the pseudospins are up and hexagons where they are down. This can be done in a consistent way because D and D_0 are supposed to be in the same sector and any closed path will necessarily cross an even number of domain walls.

(3) There is a two fold redundancy in the above prescription because the up and down hexagons can be exchanged without changing the loop pattern. Since there is no natural way to decide where is the interior and where is the exterior of a closed loop on a finite sample, a pseudospin configuration $\{\sigma_h^z=\sigma(h)\}$ and its reversed counterpart $\{\sigma_h^z=-\sigma(h)\}$ represent the same dimer covering.

This establishes a one-to-one correspondence between dimer coverings of a given topological sector and *pairs* of pseudospin sates related by a global pseudospin flip. The proof can be done in two steps.

(a) If two dimer configurations D and D' are associated with the same pseudospin state (up to a global pseudospin reversal), they are identical. The transition graph $\langle D|D'\rangle$ can be viewed as the ''difference'' between graphs $\langle D_0|D\rangle$ and $\langle D_0|D'\rangle$. This means that the $\langle D|D'\rangle$ will have loops separating regions where the pseudospins coincide in D and D' and the region where they are different. Since D and D' have the same σ^z on every hexagon, $\langle D|D'\rangle$ cannot contain any hexagon and therefore contains no loop at all.

(b) Any pseudospin configuration has a corresponding dimer state. The transition graph between D_0 and the dimer configuration we are looking for will separate $\sigma^z=+1$ hexagons from $\sigma^z=-1$ ones. The actual path of these loops will depend on D_0 but for a given reference dimerization only one such path exists. The reason for this is easily understood by looking at a single hexagon: whatever D_0 may be, there is always a single loop that surrounds this hexagon only.

We can check the above property by a direct counting. On the one hand, we have $2^{N/3}$ pseudospins configurations and $2^{N/3-1}$ pairs of nonequivalent configurations. On the other hand, there are $2^{N/3+1}$ (see Ref. 1) dimerizations on a kagome lattice with N sites and periodic boundary conditions. The agreement is found by remarking that the number of dimerizations has to be divided by 4 to get the size of a single topological sector.[64]

2. Pseudospin flip operator σ^x

One interest of the ZE pseudospin representation is that the σ_h^x operator, which flips the pseudospin at position h, can be expressed in a simple way in terms of *local* dimer operators. It seems that ZE did not realize this very useful property of their representation. The simplest dimer moves involve loops around hexagons. These 32 loops are represented in Table I. The corresponding operators

$$\hat{L}_\alpha=|L_\alpha\rangle\langle\overline{L}_\alpha|+|\overline{L}_\alpha\rangle\langle L_\alpha| \tag{A1}$$

shift the dimers along the loop L^α if it is possible and annihilate the state otherwise. We will now prove that σ^x is the sum of all the 32 kinetic operators of hexagon h:

$$\sigma^x(h)=\sum_{\alpha=1}^{32}\hat{L}_\alpha. \tag{A2}$$

The fact that this sum of dimer operators $\hat{L}^\alpha$ realizes the spin algebra is not obvious. In particular, the fact that these operators commute at two neighboring hexagons h and h' must be verified, since, in general, $[\hat{L}_\alpha(h),\hat{L}_{\alpha'}(h')]\neq 0$.

Consider an arbitrary dimerization $|D\rangle$ in the vicinity of hexagon h. The crucial point is that all the kinetic operators $\hat{L}_\alpha(h)$ but one annihilate $|D\rangle$. This is a property of the kagome lattice that we used before: for any given dimerization one and only one loop can surround hexagon h. So $|D'\rangle=\sigma^x(h)|D\rangle$ is a dimer configuration that differs from $|D\rangle$ by a single loop around h. Using the σ^z base to represent dimer coverings we know that such a state is unique and is the state obtained from $|D\rangle$ by flipping the pseudospin at h. Thus we have shown that $\sigma^x(h)\sigma^z(h)=-\sigma^z(h)\sigma^x(h)$.

One can use a very similar reasoning to show that $\sigma^x(h)$ and $\sigma^x(h')$ commute when $h\neq h'$, but this result is most easily obtained by the arrow representation.

3. Counting dimer coverings with pseudospins

The Ising basis of ZE's pseudospins provides a way of counting the number $\mathcal{N}$ of dimer coverings on any lattice K that is the medial lattice of a trivalent one. The result is

$$\mathcal{N}_{\text{dim. coverings}} = \alpha 2^{N_{\text{ps}}-1}, \tag{A3}$$

where N_{ps} is the number of pseudospins and α is the number of topological sectors, it is related to the genus by $\alpha = 2^{2g}$ in the two-dimensional cases. The factor 2^{-1} comes from the fact that a dimer configuration corresponds to two pseudospin states. Using the Euler relation we can check that Eq. (A3) indeed coincides with the result obtained with the arrow representation [Eq. (1)]:

$$\mathcal{N}_{\text{dim. coverings}} = 2^{2g} 2^{N/3+2-2g-1} = 2^{N/3+1}. \tag{A4}$$

APPENDIX B: μ KINETIC OPERATORS AND ZE PSEUDOSPINS

In order to write μ with σ^z and σ^x only, we need to express the sign $\epsilon(h)$ of Eqs. (10) and (12) in terms of the σ^z operators on the neighboring hexagons. We will do this with the help of the arrow representation. The argument generalizes easily to the $\tilde{\mu}$ operators.

First draw the arrow representation of the reference dimerization $|D_0\rangle$ in the vicinity of hexagon h, as in Fig. 12. Each neighboring hexagon of h has two arrows that belong to the star of h. These arrows can either (A_1) point toward the exterior of h, (A_2) point toward the interior of h, or (B) point in two different directions. In Fig. 12, for example, we have no hexagon in case A_1, two in case A_2, and four in case B. First look at the change in $n_{\text{out}}(h)$ when a single neighboring pseudospin is flipped with respect to the reference configuration (it has $\sigma^z = -1$). If the corresponding hexagon is of type A_1 (A_2), $n_{\text{out}}(h)$ is decreased (increased) by 2 units. If that hexagon is of type B, $n_{\text{out}}(h)$ is unchanged. On a state where a single pseudospin is down, we have, therefore, showed that $\epsilon(h) = \epsilon_{\text{ref}}(h) \Pi_{i \in A_{\text{ref}}(h)} \sigma^z(i)$ where $A_{\text{ref}}(h)$ is the set of the n eighbors of h that are of type A_1 or A_2 in the reference dimerization. $\epsilon_{\text{ref}}(h)$ is the value of $\epsilon(h)$ in the reference state.

Now look at the value of $\epsilon(h)$ when the neighboring pseudospins are in an arbitrary state $\sigma^z(h_i) = \pm 1$. If two pseudospins are flipped on hexagons that are themselves first neighbors, one arrow is flipped twice and therefore remains unchanged. This adds to $\epsilon(h)$ a -1 factor, which multiplies the single pseudospin factor discussed above. This can be seen on the example of Fig. 12. If the pseudospin of the hexagon containing the sites $(2',3,3')$ (type A_2) is flipped, the sign $\epsilon(h)$ changes; but if hexagon $(1',2,2')$ (type B) is flipped, $\epsilon(h)$ is not affected. However, if *both* hexagons are flipped, $\epsilon(h)$ is unchanged too. In addition to the $\sigma^z(h_i)$ factors coming from hexagons belonging to $A_{\text{ref}}(h)$, we must add a -1 contribution for each *pair of consecutive pseudospins that are simultaneously in a* $\sigma^z(h_i) = -1$ *state*. Such a factor is given by

$$\prod_{i=1}^{6} f[\sigma^z(h_i), \sigma^z(h_{i+1})], \tag{B1}$$

where f is equal to -1 when the two pseudospins are both down $\sigma^z(h_i) = \sigma^z(h_{i+1}) = -1$ and 1 otherwise. The product runs over the six neighbors h_i of h numerated in a cyclic way. f can be explicitly written as a polynomial:

$$f[\sigma_1^z, \sigma_2^z] = \tfrac{1}{2}(1 + \sigma_1^z + \sigma_2^z - \sigma_1^z \sigma_2^z). \tag{B2}$$

We eventually have an expression for $\epsilon(h)$ as a polynomial of ZE pseudospins operators located on neighbors of h:

$$\epsilon(h) = \epsilon_{\text{ref}}(h) \prod_{i \in A\text{ref}(h)} \sigma^z(i) \prod_{i=1}^{6} f[\sigma^z(h_i), \sigma^z(h_{i+1})]. \tag{B3}$$

The left-hand side is both a local and a reference-independent operator. On the right-hand side, the information on the arrows in the reference configuration is present at several places: in $\epsilon_{\text{ref}}(h)$, in the set of sites $A_{\text{ref}}(h)$, as well as in the σ^z operators. It is possible to check directly on this expression that $\epsilon(h)\sigma^x(h)$ satisfy the μ algebra.

APPENDIX C: REMOVING THE EXTENSIVE DEGENERACY

To perform the explicit diagonalization, it is useful to remove the extensive degeneracy. Let us denote by C_α, $\alpha = 1, \ldots, N_c$, the commuting and independent operators introduced in Sec. V E 5, and $c_\alpha = \pm 1$ their eigenvalues. We can decompose the Hilbert space in eigenspaces $\{c_\alpha\}$, using the projectors

$$P_{\pm}^{\alpha} = \tfrac{1}{2}(1 \pm C_\alpha).$$

It is then sufficient to work within the reduced space where c_α are all equal to 1, for example. The reduced space is then generated as follows. Consider the state $|\{s(h) = 1\}; \{I_k\}\rangle$ where all $s(h) = 1$, and the integrals of motion have some values $\{I_k\}$. This state exists, is unique, and has the property of transforming the action of $\mu(h)$ into that of $\tilde{\mu}(h)$ for all h. We project this state to the eigenspace $\{c_\alpha\} = 1$,

$$|\Omega; \{I_k\}\rangle = \prod_{\alpha} P_{+}^{\alpha} |\{s(h) = 1\}; \{I_k\}\rangle$$

and then generate the whole subspace $\{c_\alpha = 1\}$ by the action of the monomials in μ

$$\prod_{h=1}^{N_{\text{ps}}} \mu(h)^{n_h} |\Omega; \{I_k\}\rangle,$$

with $n_h = 0,1$. Roughly half of the spins can be eliminated recursively by the following procedure. For spins belonging to the A sublattice, we bring $\mu(h)$ at right using the commutation relations, we transform it in $\tilde{\mu}(h)$, which is 1 by construction. Some of the spins can be eliminated using the integrals of motion I_k. And finally, one of the spins entering a bow-tie operator can be eliminated by replacing it with the

product of the other three spins in the bow tie and the operator $T(h)$. The latter operator is brought to the right, transformed in $\tilde{T}(h)$ whose value is 1. Similarly, one can construct the eigenspace for any values of $\{c_\alpha\}$. The passage from a sector of fixed $\{c_\alpha\}$ to another can be realized by operators $\tilde{\mu}(h)$ belonging to one of the sublattices B,C,D. Since these operators commute with the Hamiltonian, the spectrum of $\mathcal{H}_\mu$ will be the same in all the sectors, which proves that the global degeneracy of the spectrum is 2^{N_c}.

The action of the Hamiltonian on the reduced basis is computed using the same procedure as above. The fact that we work in a space with dimension divided by $2^{N_{ps}/2}$ allows us to perform numerical diagonalization for relatively large systems, up to $N_{ps}=48$.

APPENDIX D: DIMER-DIMER CORRELATIONS

We show here that the eigenstates of the Hamiltonian of the μ model can be chosen to have vanishing dimer-dimer correlations beyond a few lattice spacings.

Let us consider a triangle (1,2,3) on the kagome lattice. On these three sites we may define an arrow operator a_i whose value is 1 if the corresponding arrow points toward the interior of the triangle and 0 otherwise. With this definition, the dimer occupation number n_{12} on bond (12) is $n_{12}=a_1a_2$. Now we assume that we have three operators $\hat{O}_i$ $(i=1,2,3)$, which satisfy

$$\forall i, \quad \hat{O}_i a_i = a_i \hat{O}_i, \tag{D1}$$

$$\forall i \neq j, \quad \hat{O}_i a_j = (1-a_j)\hat{O}_i, \tag{D2}$$

$$\hat{O}_i|0\rangle = \pm|0\rangle. \tag{D3}$$

These relations just mean that $\hat{O}_1$ *flips* the arrows on sites 2 and 3 but does not touch the arrow 1, etc. $|0\rangle$ is a ground-state of the model which is also an eigenvector for $\hat{O}_i$. Notice that if $\hat{O}_1$ and $\hat{O}_2$ exist, $\hat{O}_3=\hat{O}_1\hat{O}_2$ is a valid choice. Under these conditions, we show that n_i are uncorrelated with any other bond that is unaffected by the three $\hat{O}_i$. As we will explain, $\hat{O}_i$ will be realized as local combinations of $\tilde{\mu}$ and $\tilde{T}$. From Eqs. (D1) and (D2), it is simple to check that

$$n_{12}\hat{O}_3 = \hat{O}_3(1-n_{12}-n_{23}-n_{31}) \tag{D4}$$

(plus cyclic permutations). Now let X be any operator that commutes with the three $\hat{O}_i$ [later we will chose $X=1$ or $X=n_{kl}$, where (kl) is a remote bond]. Using Eqs. (D3) and (D4), the correlation $\langle Xn_{ij}\rangle$ becomes

$$\langle Xn_{12}\rangle = \langle 0|Xn_{12}(\hat{O}_3)^2|0\rangle \tag{D5}$$

$$= \langle 0|\hat{O}_3 X(1-n_{12}-n_{23}-n_{31})\hat{O}_3|0\rangle \tag{D6}$$

$$= \langle X\rangle - \langle Xn_{12}\rangle - \langle Xn_{23}\rangle - \langle Xn_{31}\rangle. \tag{D7}$$

Using the relations obtained by cyclic permutations and solving the three linear equations we find

$$\langle Xn_{ij}\rangle = \tfrac{1}{4}\langle X\rangle. \tag{D8}$$

Using $X=1$ we get that the dimer density is $\frac{1}{4}$ and using $X=n_{kl}$ (a remote link) we find

$$\langle n_{kl}n_{ij}\rangle = \tfrac{1}{16} = \langle n\rangle^2. \tag{D9}$$

In order to complete the demonstration we still have to show that operators $\hat{O}_i$ can be constructed for any triangle. Let the state $|0\rangle$ be an eigenstate of $\tilde{\mu}(a\in A)$ and $\tilde{T}(b\in B)$ described in the preceding section. Depending on its position, relative to the four sublattices *A*, *B*, *C* and *D*, a triangle (123) (on kagome) will demand slightly different constructions for its $\hat{O}_i$ operators. For brevity, we will only consider the case of a triangle located between a hexagon $a\in A$ and a hexagon $b\in B$. It generalizes straightforwardly to the other cases. Let $i=1$ be the common site of hexagons a and b, $i=2\in a$ and $i=3\in b$. It can be checked that the following choice satisfies Eqs. (D1) and (D2):

$$\hat{O}_1 = \tilde{T}(b) \tag{D10}$$

$$\hat{O}_2 = \tilde{\mu}(a)\tilde{T}(b) \tag{D11}$$

$$\hat{O}_3 = \tilde{\mu}(a) \tag{D12}$$

The result given Eq. (D9) shows that dimer-dimer correlations are extremely short ranged.[65]

APPENDIX E: FERMIONIC REPRESENTATION AND INTEGRALS OF MOTION

Integrals of motion. Let us analyze the case of closed systems with the topology of the torus, which is the geometry we used for the numerical diagonalization. The lattice on which the μ operators live is triangular and it is made by the centers of hexagons of the kagome lattice. We call m_1, m_2, m_3 the number of closed lines in each elementary direction on the lattice, having length n_1, n_2, n_3 respectively,[66] so that $N_{ps}=m_1n_1=m_2n_2=m_3n_3$. We denote by M the total number of such lines, $M=m_1+m_2+m_3$. We label by L_k, $k=1,\ldots,M$ the closed straight lines on the triangular lattice, and l_k and l_{k+1} the lines on the corresponding kagome lattice bordering the line L_k (with obvious periodicity conditions). Associated with each kagome line l_k, we can define the following operators

$$\Gamma_k = \prod_{j\in l_k}^{\rightarrow} \gamma_j, \quad \tilde{\Gamma}_k = \prod_{j\in l_k}^{\leftarrow} \tilde{\gamma}_j,$$

where the products run over the sites j of the kagome line l_k, with some ordering indicated by the arrow. Since every line l_k visits any hexagon zero or two times, operators Γ_k and $\tilde{\Gamma}_k$ commute with all the operators $\mu(h)$ and $\tilde{\mu}(h)$. From the correspondence with the dimer states, we know that Γ_k and $\tilde{\Gamma}_k$ correspond to dimer moves on nontrivial loops around the torus, so they change the topological sector.[67]

In each topological sector we can construct the following integrals of motion, associated with the closed straight lines L_k on the triangular lattice:

$$I_k=(-i)^n\Gamma_k^{\rightarrow}\Gamma_{k+1}^{\leftarrow}=\prod_{h\in L_k}^{\rightarrow}\mu(h),$$

$$\tilde{I}_k=(-i)^n\tilde{\Gamma}_{k+1}^{\rightarrow}\tilde{\Gamma}_k^{\leftarrow}=\prod_{h\in L_k}^{\leftarrow}\tilde{\mu}(h),$$

where n denotes the number of hexagons on L_k and the arrows denote the ordering in $\Gamma_k,\tilde{\Gamma}_k$. The third member of both equalities is invariant by circular permutation of the sites on the line L_k.

The two sets of integrals of motion $\{I_k\}$, $\{\tilde{I}_k\}$ are not independent. To check this, we use the commuting variables

$$s(h)=\mu(h)\tilde{\mu}(h),$$

measuring the parity number of fermions around the hexagon h,

$$s(h)=\prod_j \gamma_j\tilde{\gamma}_j=(-i)^6\prod_j (1-2n_j).$$

Then,

$$I_k\tilde{I}_k=(-1)^n\prod_{h\in L_k} s(h)=(-1)^n,$$

where the last equality is a consequence of the constraint on the fermion number around the two types of kagome triangles. Moreover, integrals of motion corresponding to the L_k lines with the same orientation on the lattice are not all independent,

$$\prod_{k=1}^{m_1} I_k=(-i)^{m_1n_1}=(-i)^{N_{\rm ps}}, \tag{E1}$$

and similarly for the other two orientations. Such a constraint on physical states is not unexpected, since the product of the lines with some orientation contains all the operators $\mu(h)$ exactly once, that is, all the operators γ_i twice, so it has to be proportional to the identity.

In conclusion, there are at most $M-3$ independent integrals of motion, where M is the number of different closed straight lines one can draw on the triangular lattice wrapped on the torus (in some cases, the $M-3$ lines are not independent and some of the quantities I_k can be written as products of the others).

Basis for the Hilbert space. The commuting quantities $s(h)$ and I_k can be used to label the states in the Hilbert space. Let us first check that we obtain the right dimension. Due to the $M-2$ independent constraints $\Pi_{h\in L_k}s(h)=1$, only $N_{\rm ps}-(M-2)$ of the operators $s(h)$ are independent. Both type of operators, $s(h)$ and I_k, can take only two values, ± 1, or $\pm i$ for I_k on a line of odd length. Taking into account the topological degeneracy, the number of states in the Hilbert state is $4\times 2^{N_{\rm ps}-(M-2)}\times 2^{M-3}=2^{N_{\rm ps}+1}$, which is the right dimension of the dimer space (in the case when there are extra relations between the lines L_k, the number of independent integrals of motion and the number of constraints on $s(h)$ are diminished by the same number).

*Electronic address: gmisguich@cea.fr
†Electronic address: serban@spht.saclay.cea.fr
‡Electronic address: vpasquier@cea.fr

[1] V. Elser, Phys. Rev. Lett. **62**, 2405 (1989).
[2] C. Zeng and V. Elser, Phys. Rev. B **42**, 8436 (1990).
[3] J.T. Chalker and J.F.G. Eastmond, Phys. Rev. B **46**, 14 201 (1992).
[4] R.R.P. Singh and D.A. Huse, Phys. Rev. Lett. **68**, 1766 (1992).
[5] V. Elser and C. Zeng, Phys. Rev. B **48**, 13 647 (1993).
[6] C. Zeng and V. Elser, Phys. Rev. B **51**, 8318 (1995).
[7] J.B. Marston and C. Zeng, J. Appl. Phys. **69**, 5962 (1991).
[8] S. Sachdev, Phys. Rev. B **45**, 12 377 (1992).
[9] P.W. Leung and V. Elser, Phys. Rev. B **47**, 5459 (1993).
[10] N. Elstner and A.P. Young, Phys. Rev. B **50**, 6871 (1994).
[11] T. Nakamura and S. Miyashita, Phys. Rev. B **52**, 9174 (1995).
[12] P. Tomczak and J. Richter, Phys. Rev. B **54**, 9004 (1996).
[13] P. Lecheminant, B. Bernu, C. Lhuillier, L. Pierre, and P. Sindzingre, Phys. Rev. B **56**, 2521 (1997).
[14] C. Waldtmann, H.U. Everts, B. Bernu, C. Lhuillier, P. Sindzingre, P. Lecheminant, and L. Pierre, Eur. Phys. J. B **2**, 501 (1998).
[15] F. Mila, Phys. Rev. Lett. **81**, 2356 (1998).
[16] B.H. Bernhard, B. Canals, and C. Lacroix, Phys. Rev. B **66**, 104424 (2002).
[17] Kagome comes from the Japanese words ''kago'' (basket) and ''me'' (eye). Although it is often written with a capital K and an accent on the e in the literature, the appropriate spelling for a Japanese common noun is *kagome*.
[18] D.S. Rokhsar and S.A. Kivelson, Phys. Rev. Lett. **61**, 2376 (1988).
[19] R. Moessner, S.L. Sondhi, and E. Fradkin, Phys. Rev. B **65**, 024504 (2002).
[20] P.W. Kasteleyn, J. Math. Phys. **4**, 287 (1963).
[21] G. Misguich, D. Serban, and V. Pasquier, Phys. Rev. Lett. **89**, 137202 (2002).
[22] R. Moessner and S.L. Sondhi, cond-mat/0212363 (unpublished).
[23] R. Moessner and S.L. Sondhi, Phys. Rev. Lett. **86**, 1881 (2001).
[24] R. Moessner, S.L. Sondhi, and P. Chandra, Phys. Rev. B **64**, 144416 (2001).
[25] R.J. Baxter, J. Math. Phys. **11**, 784 (1970).
[26] D.A. Huse and A.D. Rutenberg, Phys. Rev. B **45**, 7536 (1992).
[27] J.T. Chalker, P.C.W. Holdsworth, and E.F. Shender, Phys. Rev. Lett. **68**, 855 (1992).
[28] This is, in fact, a general property of lattices made of corner-sharing triangles, which are precisely the lattices we consider in this paper.
[29] We use the following units for the Hamiltonian: $\mathcal{H}=2J\Sigma_{\langle i,j\rangle}\vec{S}_i\cdot\vec{S}_j$.
[30] Although the gauge degrees of freedom appearing in the Sp($2N$) formulation correspond to singlet excitations, such states are expected to acquire a (possibly small) gap.

[31] First studies used the value of the singlet-triplet gap (spin gap) as the energy window. The fate of the spin gap in the kagome Heisenberg antiferromagnet is not completely settled, although numerical results suggest a small but nonzero spin gap in the thermodynamic limit (Ref. 14) We note that a vanishing spin gap would cast some doubt on the validity of the short-range RVB approach to that spin model. Provided that the gap has a smooth behavior with the system size, this does not prevent one from using the gap as an energy window to estimate the entropy.

[32] P. Sindzingre, G. Misguich, C. Lhuillier, B. Bernu, L. Pierre, Ch. Waldtmann, and H.-U. Everts, Phys. Rev. Lett. **84**, 2953 (2000).

[33] B. Bernu and G. Misguich, Phys. Rev. B **63**, 134409 (2001).

[34] G. Misguich and B. Bernu (unpublished).

[35] Take the infinite volume limit before taking the temperature to zero.

[36] M. Mambrini and F. Mila, Eur. Phys. J. B **17**, 651 (2000).

[37] Zeng and Elser did not consider all dimer coverings but restricted their study to one topological sector. This has no consequence in the thermodynamic limit, but it is an approximation on finite-size systems. For this reason their results differ from those of Mambrini and Mila who worked in the full dimer space.

[38] D.S. Rokhsar, Phys. Rev. B **42**, 2526 (1990).

[39] We repeat the fit when one and when any two data points are removed. The minimum and maximum values of the coefficient are used to estimate the uncertainty.

[40] A.P. Ramirez, B. Hessen, and M. Winklemann, Phys. Rev. Lett. **84**, 2957 (2000).

[41] Ch. Waldtmann, H. Kreutzmann, U. Schollwöck, K. Maisinger, and H.-U. Everts, Phys. Rev. B **62**, 9472 (2000).

[42] R. Siddharthan and A. Georges, Phys. Rev. B **65**, 014417 (2002).

[43] P. Tomczak and J. Richter, J. Phys. A: Math. Gen. **36**, 5399 (2003).

[44] A. Voigt, J. Richter, and P. Tomczak, Physica A **299**, 107 (2001).

[45] This move should not, however, contain topologically nontrivial loops.

[46] B. Sutherland, Phys. Rev. B **37**, 3786 (1988).

[47] A dimer on bond ij oriented from i to j then corresponds to $(|\uparrow_i\downarrow_j\rangle - |\uparrow_j\downarrow_i\rangle)/\sqrt{2}$.

[48] Notice the difference with bipartite lattices where it is possible to orient the bonds so that the sign $\langle a|b\rangle$ is always be positive (Ref. 46).

[49] The length $L_{\max}$ of longest loop around a star is always even in our family of lattices since $L_{\max}=2L_{\min}$. For this reason Eq. (12) is valid for any such lattices.

[50] S. Sachdev, *Quantum Phase Transitions*, (Cambridge University Press, New York, 1999).

[51] M. Mambrini, J. Trébosc, and F. Mila, Phys. Rev. B **59**, 13 806 (1999).

[52] J. Vidal, R. Mosseri, and B. Douçot, Phys. Rev. Lett. **81**, 5888 (1998).

[53] It is not surprising to find such a three-sublattice order in this variational approximation since the translation invariance is explicitly broken by Eq. (34).

[54] They are not all independent on a finite system with periodic boundary conditions, in the sense that some products on closed straight lines reduce to products of the integrals of motion (monomials in the μ operators—the I_k defined below). The number of dependent operators goes as the number of lines $M\sim\sqrt{N_{\rm ps}}$, so in the thermodynamic limit they represent a negligible fraction of the total number of commuting operators. The degeneracy of the spectrum will be 2^{N_c}, of the order of $2^{N_{\rm ps}/2}$

[55] It turns out that, as a finite-size effect, the $N_{\rm ps}=12$ and 16 systems also exactly have $\langle\mu\rangle=-\frac{1}{2}$ in their ground state.

[56] Three or six depending on whether or not the axis symmetry is also spontaneously broken.

[57] G. Santoro, S. Sorella, L. Guidoni, A. Parola, and E. Tosatti, Phys. Rev. Lett. **83**, 3065 (1999).

[58] The Quantum Hall Effect, edited by R.E. Prange and S. M. Girvin (Springer, New York, 1987).

[59] If one first neglects the hard-core repulsion of dimers, one can build a state where all the dimers are in the same zero-momentum wave function $\phi(r)=1$. The many-dimer wave function is of course $\psi(r_1,\ldots,r_n)=\phi(r_1)\ldots\phi(r_n)=1$ (already symmetrized) whatever the dimer positions $r_1,\cdots,r_n$ are. Projecting this state (Gutzwiller-like) onto the space of no double occupancy precisely gives the equal-amplitude superposition of all fully packed dimer configurations.

[60] C.L. Kane, S. Kivelson, D.H. Lee, and S.C. Zhang, Phys. Rev. B **43**, 3255 (1991).

[61] M.V. Feigel'man and M.A. Skvortsov, Nucl. Phys. B **506**, 665 (1997).

[62] A. Paramekanti, L. Balents, and M.P.A. Fisher, Phys. Rev. B **66**, 054526 (2002).

[63] L. Balents and A. Paramekanti, cond-mat/0212589 (unpublished).

[64] It is a property of the kagome lattice that the four topological sectors have exactly the same dimension.

[65] For Eq. (D9) to hold, the two bonds must be at a large enough distance so that $\tilde{\mu}$ and $\tilde{T}$ involved in the $\hat{O}_i$ of one triangle do not touch the second triangle. This condition is automatically satisfied beyond six kagome-lattice spacings.

[66] We do not consider the special case when one of the lines has length 2.

[67] Two operators Γ_k and Γ_r anticommute if they correspond to two independent cycles, so we can choose Γ_k and $\tilde{\Gamma}_r$ to generate the four topological sectors on the torus.